Reviews in Mineralogy & Geochemistry
Vol. 63, pp. 27-57, 2006

Neutron Production, Neutron Facilities and Neutron Instrumentation

Sven C. Vogel
Los Alamos Neutron Science Center
Los Alamos National Laboratory
Los Alamos, New Mexico, 87545, U.S.A
e-mail: sven@lanl.gov

Hans-Georg Priesmeyer
Geesthacht Neutron Scattering Facility
GKSS Research Center
21502 Geesthacht, Germany
e-mail: hans-georg.priesmeyer@gkss.de

NEUTRON GENERATION

The main natural source of free neutrons is secondary radiation from *cosmic radiation* (creation of particles by interactions of cosmic radiation particles with atoms of the earth's atmosphere). The main sources of neutrons generated artificially are nuclear reactors. Free neutrons have an average lifetime of about 888 seconds (e.g., Mampe et al. 1989a,b: 887.6 ± 3 s) and decay according to

$$n \rightarrow p + e^- + \overline{\nu} \quad (1)$$

into a proton p, an electron e^- and an anti-neutrino $\overline{\nu}$. Hence, free neutrons must be produced shortly before their use. Besides reactors, where neutrons from nuclear fission reactions after moderation induce further nuclear fissions in a chain reaction, neutrons for research may be generated by a process called spallation. Neutron sources based on these two concepts as well as some special cases of neutron generation are described in more detail below. Figure 1 shows the historical evolution of the performance of neutron sources. In all cases it should be noted that the neutron flux (number of neutrons per unit area and unit time) at the sample is much lower than the peak flux provided by the source. For instance, the spallation neutron source at LANSCE (Los Alamos Neutron Science Center, Los Alamos, U.S.A.) produces 10^{16} neutrons cm^{-2} s^{-1}, but at the HIPPO instrument, with a moderator to sample distance of 9 m, only a flux of 2.4×10^7 neutrons cm^{-2} s^{-1} is available for neutron energies in the "thermal" (< ~0.4 eV) range (see below) suitable for diffraction. Other facilities provide thermal neutron fluxes of similar magnitude. From these low intensities, as compared to the number of atoms in a cubic centimeter of solid material, it is apparent that the radiation damage from thermal neutrons for most materials is negligible, even for days of exposure.

Reactor sources

Nuclear reactors have been, and continue to be, an important and reliable source of neutrons as a research tool with wide application in different scientific fields. Most research reactors allow user access for neutron scattering experiments, with instrumentation that has greatly evolved since the early days of this technique (Shull 1995). As expensive scientific facilities, they tend to be multi-purpose (nuclear physics, nuclear engineering, diffraction, etc.), and many reactors have been operating for more than 30 years.

1529-6466/06/0063-0002$05.00 DOI: 10.2138/rmg.2006.63.2

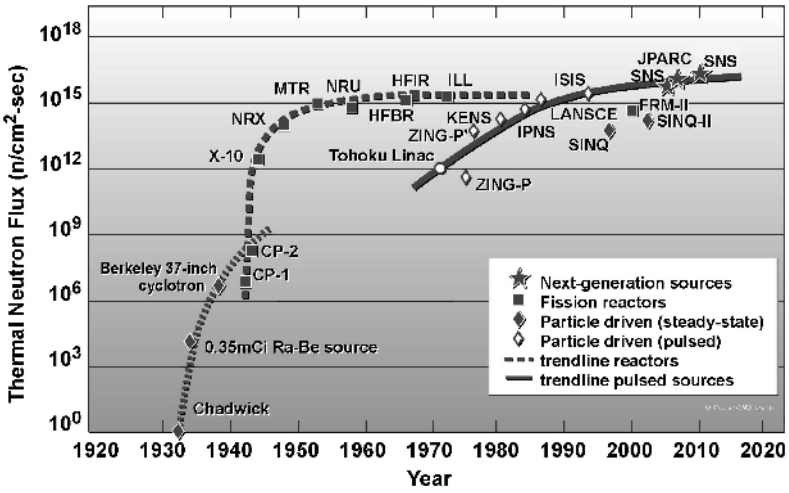

Figure 1. Historical evolution of the performance (peak thermal neutron flux) of neutron sources over time. The Spallation Neutron Source (SNS) has two data points, representing the initial power level and that after the upgrade (Mason et al. 2003).

Nuclear reactors operate on the physical basis of the *fission chain reaction*. In heavy nuclei, such as uranium, the number of neutrons exceeds the number of protons by about 40%. Figure 2 shows a schematic of the fission process. When a neutron is absorbed, for instance, by a ^{235}U nucleus (Fig. 2A), a large amount of energy is transferred into the system. The excited ^{236}U compound nucleus begins to oscillate (Fig. 2B) with increasing amplitude (Fig. 2C), until the repelling Coulomb force drives it into separation (Fig. 2D). Each fission liberates 2 or 3 free neutrons, so that a chain reaction becomes possible. One of these neutrons is definitely required to maintain the chain reaction and, thus, trigger the release of the next generation of neutrons. The number of neutrons produced in a nuclear reactor scales with its thermal energy production: each fissioning nucleus produces energy of about 200 MeV. Thus, approximately 3×10^{16} fission events per second occur per 1 MW reactor power, resulting in about 7.5×10^{16} neutrons per second per MW.

In a research reactor, as many neutrons as possible should be available for the experiments. Careful design of the reactor core and sophisticated neutron optical devices are needed to

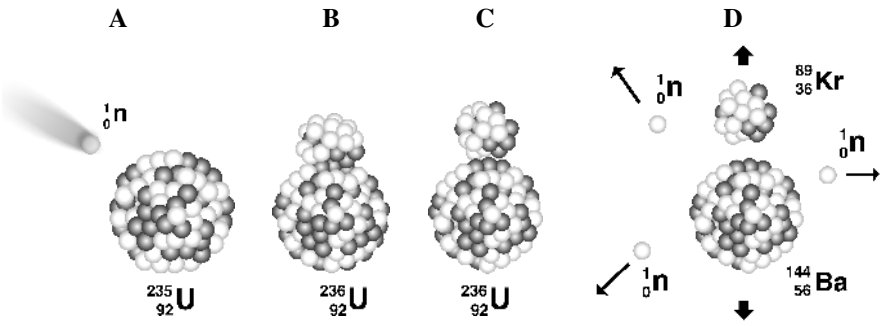

Figure 2. The fission process.

maximize the flux of neutrons at the sample positions of the specific experiments. This requires a very high power density in the reactor core and, therefore, special design features like a compact core and reflectors to reduce neutron loss from the core. Numerous designs of research reactors were developed in the early days of the technology; of these designs the *pool* and *tank type* reactors became the most common ones (Bauer and Thamm 1991). The core of such reactors is a group of fuel elements in a large pool of light or heavy water (^1H_2O or $^2H_2O = D_2O$, respectively). Movable rods containing neutron-absorbing materials like boron or cadmium are distributed among the fuel elements in order to control the fission process by absorbing neutrons and, hence, slowing down the chain reaction. Water moderates (decelerates) the neutrons and cools the reactor, while graphite or beryllium are generally used as reflector materials, reflecting neutrons back into the reactor core. Beam tubes to extract the neutrons from the core region are inserted in the wall of the pool or tank. Figure 3 shows a schematic of the FRM-2 research reactor in Munich, Germany, with the fuel element and control rod in the center of the reactor core and the horizontal beam tubes leading to the instruments. The operation of this modern reactor started in 2004. For safety purposes, the FRM-2 reactor has two independent mechanisms for controlled shutdown of the reactor under all circumstances. The control rod, made of highly neutron absorbing material, is located in the hollow fuel element and controls the reactor power via the amount of control rod area exposed to neutron emitting uranium. It can be decoupled from its driving device to fall down and completely shield the fuel element, hence, stopping the chain reaction. The second, independent shutdown mode are five highly neutron absorbing hafnium shut down rods in the moderator tank of the reactor core. During normal operation, these rods are fully withdrawn. When activated, they drop into positions close to the core and end the chain reaction by absorbing neutrons. Four out of the five rods are sufficient to keep the reactor subcritical, i.e., prevent the chain reaction. Note that both shutdown systems rely on gravity, i.e., they are operational without electrical power. Also note that the neutron beam tubes do not provide a direct sight to the reactor core, markedly reducing the fast neutron and gamma radiation backgrounds (FRM-2 2004). The reactor fuel elements are typically rods of urania (UO_2) of several cm in diameter. Each fuel rod is embedded in a steel or Zircaloy tube (cladding).

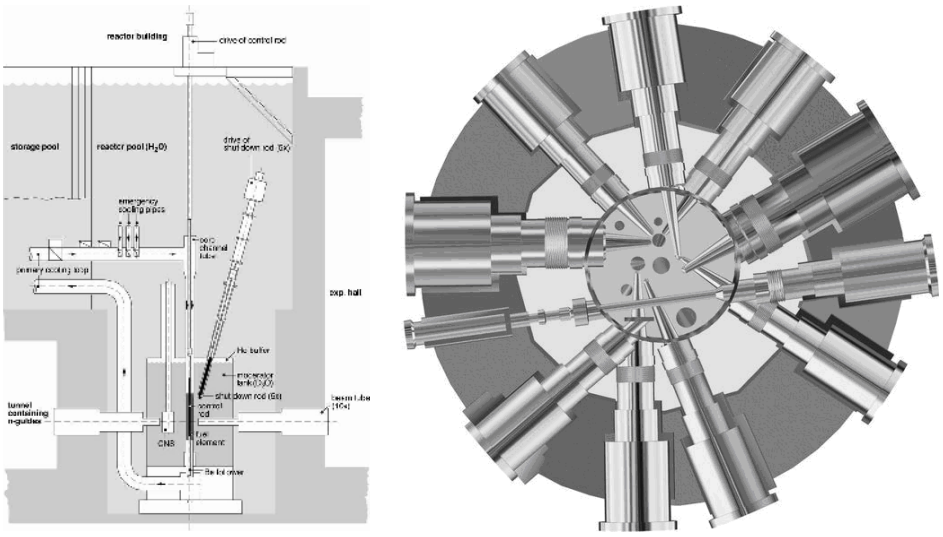

Figure 3. Simplified vertical (left) and horizontal (right) sections of the research reactor FRM-2 at Munich, Germany. The internal diameter of the reactor pool is approximately 5 m (FRM-2 2004).

Neutrons within a reactor have a broad energy distribution, which extends from below 0.001 eV to more than 10 MeV and can roughly be divided into three subgroups:

- Neutrons with energies above 500 keV are called "*fast neutrons*." They originate from the fission process and their spectral distribution may be approximated by

$$N(E) \propto e^{-E} \sinh\sqrt{2E} \quad (E \text{ in MeV}) \tag{2}$$

- The "*epithermal* range" of neutron energies extends from approximately 200 meV up to 500 keV. In this range, the neutron spectrum is primarily determined by the slowing down process by elastic collisions of the neutrons with moderator nuclei, resulting in a spectral distribution

$$N(E) \propto \frac{1}{E} \tag{3}$$

- Below 200 meV the spectral distribution of the neutrons looks like one of a gas in equilibrium with the thermal motion of the moderator nuclei, resulting in a *Maxwellian distribution*

$$N(E) \propto \frac{E}{k_B T} \cdot e^{-E/k_B T} \tag{4}$$

  Neutrons with this energy spectrum are called "*thermal neutrons*." The average neutron energy emitted from a water moderator at room temperature is 25 meV, corresponding to a neutron wavelength of 0.18 nm.

In general, the absolute intensity of each of these three components depends on the reactor type, the reactor power and the location within the reactor core, with a maximum near the center of the active zone of the core. Some applications, such as small-angle scattering, require neutron energies even below the thermal region. Such neutrons are termed "*cold neutrons*." They emerge from a so-called *cold source*, which, in fact, is not a source that creates new neutrons, but rather a hydrogenous low-temperature moderator. The neutron wavelength is thereby changed to 0.5 nm and longer.

Since neutrons have become a unique tool to study the structure and dynamics of materials at the atomic level, neutron scattering plays a dominant role among the experimental methods utilized at research reactors. Being electrically neutral, neutrons, unlike charged particles, are not scattered by the electron clouds surrounding the atoms, and thus may penetrate through considerable thickness of material layers. This allows the investigation of bulk samples under differing environmental conditions such as high pressure, high or low temperature, or strong magnetic fields (see below). Figure 4 illustrates the large number of instruments available at the Institut Laue-Langevin (ILL) in Grenoble, France, the world's largest research reactor.

Scattering and absorption of neutrons are competing nuclear processes, whose fractional ratios differ from isotope to isotope. This feature is often used in research reactors to produce radioisotopes. Since almost all materials irradiated by neutrons become radioactive to a certain extent, safe handling of specimens after an experiment is to be assured by health physics measurements. Since the gamma radiation emitted by the nuclei in the sample after neutron capture is characteristic for every nuclide, it is possible to trace elements in the range of parts per billion (ppb). This has led to the installation of equipment into research reactors that allows for so-called neutron activation analysis. At most research reactors, facilities are set up to do neutron radiography (see below and Winkler 2006, this volume) in two or three spatial dimensions. This method may be considered to be complementary to X-ray imaging, because the systematic dependence of transmission contrast prevailing for X-rays does not exist in the case of neutrons. Hence, light elements (especially hydrogenous materials) can be identified and visualized, even if they are embedded within heavy structures.

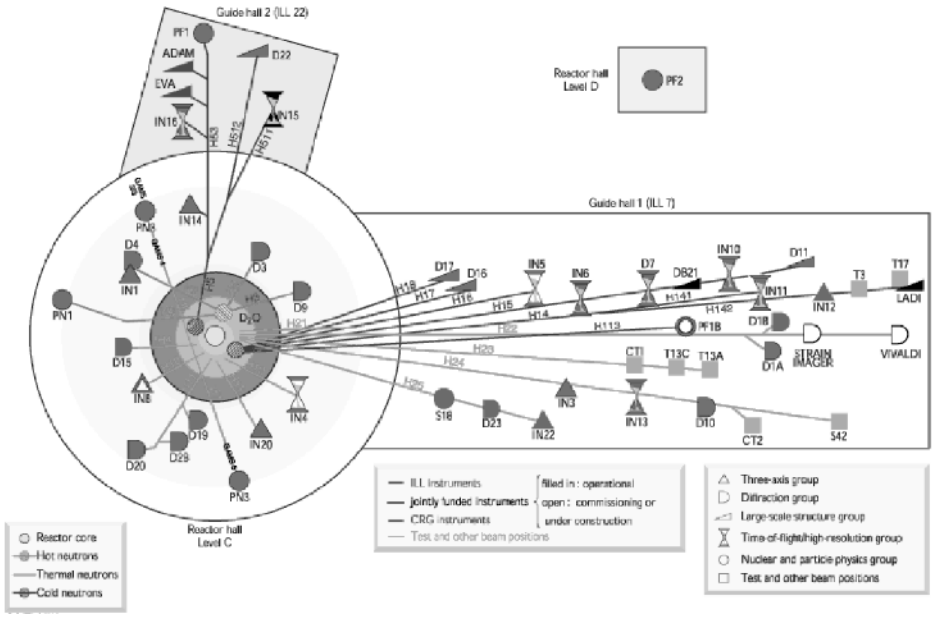

Figure 4. Floor plan of the experimental halls at the Institut Laue-Langevin (ILL), the world's largest research reactor (ILL 2004). ILL (2004) Insititut Laue-Langevin website: *http://www.ill.fr*

The International Atomic Energy Agency keeps track of the international development of research reactor history, which is documented in their research reactor database (*http://www.iaea.org/worldatom/rrdb*).

Spallation sources

For spallation, hydrogen ions with no electron (proton, H^+) or two electrons (H^-) are produced by an ion source and accelerated in vacuum to energies of typically 800 MeV (corresponding to about 84% of the speed of light) and directed to a heavy-metal target (e.g., uranium at the ISIS spallation source in Chilton, U.K., or tungsten at the LANSCE spallation source in Los Alamos, U.S.A.). In a linear accelerator (linac), the ions are accelerated in stages by a standing electric wave (i.e., the points of zero field, the nodes, do not change their location) in a RF (radio frequency) cavity. So-called drift tubes shield the ions from the field when the direction of the electric field would decelerate the ions. In each gap between drift tubes, the ions gain energy and become faster, hence, the length of the drift tubes and gaps has to increase with the ion energy. When the direction of the field has reversed, ions of the opposite charge are accelerated in the gaps, increasing the efficiency of the system. Magnetic fields are used to focus and bunch the ions at the end of each drift tube. The acceleration process for a linear accelerator of this type is illustrated in Figure 5 with H^+ ions being accelerated in the gaps between the drift tubes by the positive half-wave. At this point, the H^- ions travel in the drift tubes and are shielded from the field (H^- ions are not shown in Figure 5). 2.49 ns later (half the period of the 201 MHz frequency wave), the field will have the opposite sign and the H^- ions will be accelerated in the gaps between the drift tubes. At LANSCE, the second stage of the linear accelerator consists of 165 gaps and accelerates the ions to 40% of the speed of light. Another type of accelerator is the synchrotron. At spallation sources both types may be used in combination. Stripper foils are used to remove the electrons from the H^- ions.

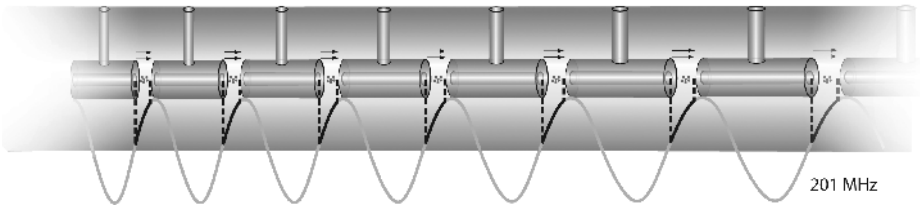

Figure 5. Schematic of a section of the LANSCE accelerator showing the acceleration of protons. The length of the drift tubes and the gaps between the drift tubes are not to scale.

At LANSCE, the positive hydrogen ions, stripped of their electrons, are then injected into a 30-m-diameter Proton Storage Ring (PSR). The PSR converts a 625-μs pulse of negative hydrogen ions into a 125 ns intense burst of protons, which is guided to the spallation target. Proton currents at the brightest spallation sources currently available are 125 μA at LANSCE and 200 μA at ISIS. Figure 6 shows a schematic of the LANSCE target. LANSCE has a split target, consisting of upper and lower targets with the proton beam hitting both targets vertically. Both targets are tungsten cylinders with 10 cm diameter and 7.25 cm and 27 cm length for the upper and lower target, respectively. Even though a so-called slab moderator in a single target piece configuration generates about a factor of two higher thermal flux than a so-called flux-trap moderator, which views the gap between the two targets in split target goemetry, this gain is degraded by the fact that a slab moderator in single target configuration produces about a factor of 20 more high energy neutrons, which comesfrom viewing the target directly. Because of that, the signal to noise ratio favors the flux-trap moderator with the split target configuration. The target-moderator-reflector-shielding (TMRS) module is located in the center of a 3.7 m thick laminated iron/concrete biological shield.

The proton bursts are released from the storage ring to the target 20 (LANSCE) or 50 (ISIS) times per second. When the target is hit by the protons, target nuclei are spalled ("smashed") into many small particles (contrary to fission where basically two nuclei of roughly the same

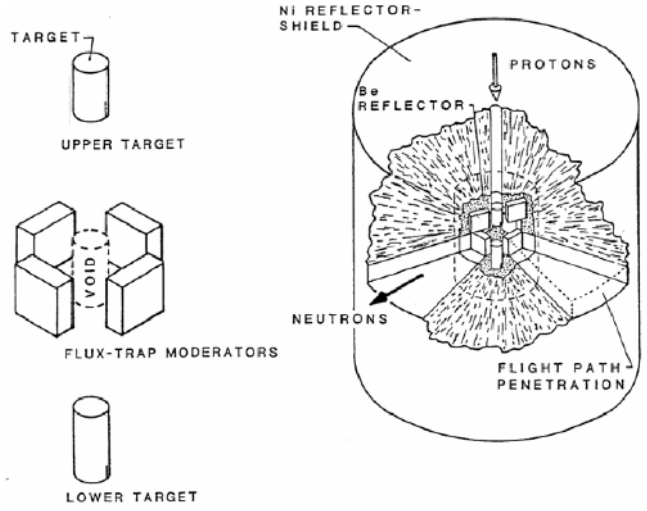

Figure 6. Schematic of the LANSCE target-moderator configuration (Lisowski et al. 1990).

mass and few neutrons are generated) (Windsor 1981, Section 2.2.). Figure 7 shows a schematic of the spallation process: When a pulse of energetic protons (bright grey) hits a tungsten target, each proton that collides with a tungsten nucleus as in (a) causes the nucleus to release ~20 neutrons (dark grey) with different energies, represented by different grey-scales in (b). Moderated neutrons traveling in a particular direction move along a beam line (c). The resulting pulse of neutrons is very short, but as the pulse travels down the beam line, with the higher energy neutrons traveling faster, the pulse stretches out in space, and the arrival times of the neutrons serve to identify their energies and wavelengths (time-of-flight method, as discussed below).

Neutrons generated by spallation in the targets drive the moderator-reflector configuration (Fig. 8). Beryllium has a large neutron scattering cross-section with negligible absorption and is therefore used as a neutron reflector. Moderators slow down the spallation neutrons and are at LANSCE 13 by 13 cm^2 in area and 2.5 cm thick. Three of the LANSCE moderators are ambient temperature water moderators, the fourth is liquid parahydrogen at 20 K. The modular design with target, moderators and reflectors in one unit (Fig. 8, left) allows for changing the entire target/moderator system within 3 weeks, schematically shown in the right part of Figure 8. The proton beam enters the TMRS module from the top, guided by the 90° bending magnets.

As can be seen in Figure 9, in particular the LANSCE accelerator serves as a versatile tool for various scientific applications besides neutron generation for scattering, ranging from proton radiography (King et al. 1999) to nuclear physics and medicine (Lisowski 2005).

The sources at ISIS and LANSCE produce neutron fluxes on the order of 10^{16} neutrons cm^{-2} s^{-1}. Spallation neutron sources have, compared to reactor sources, the advantage that

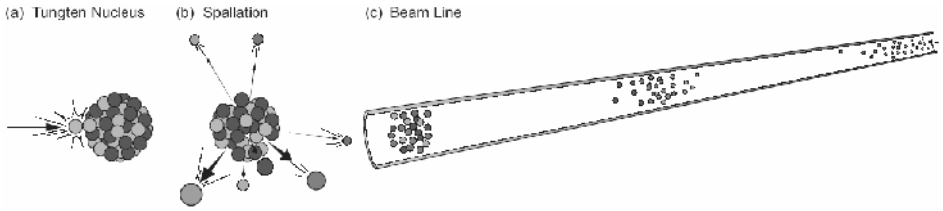

Figure 7. The spallation process (Hurd and Schaefer 2006).

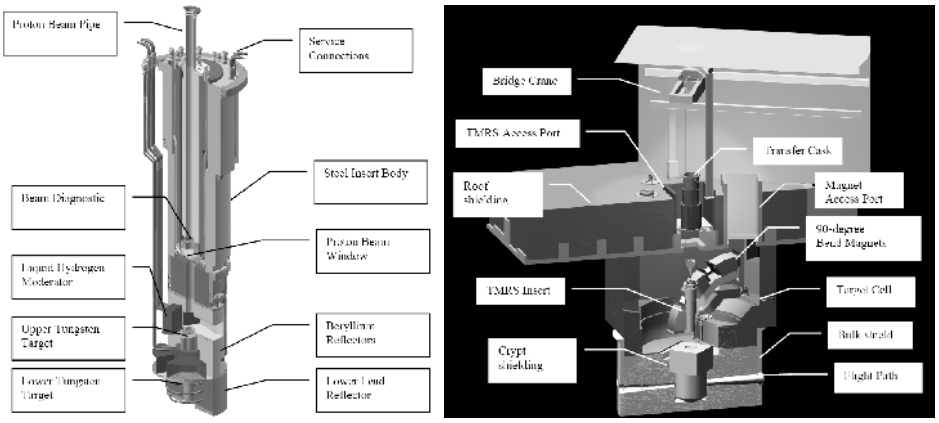

Figure 8. Cutaway view of the LANSCE target-moderator-reflector-shielding (TMRS) module (left) and exchange of the TMRS module (right, Donahue et al. 1999).

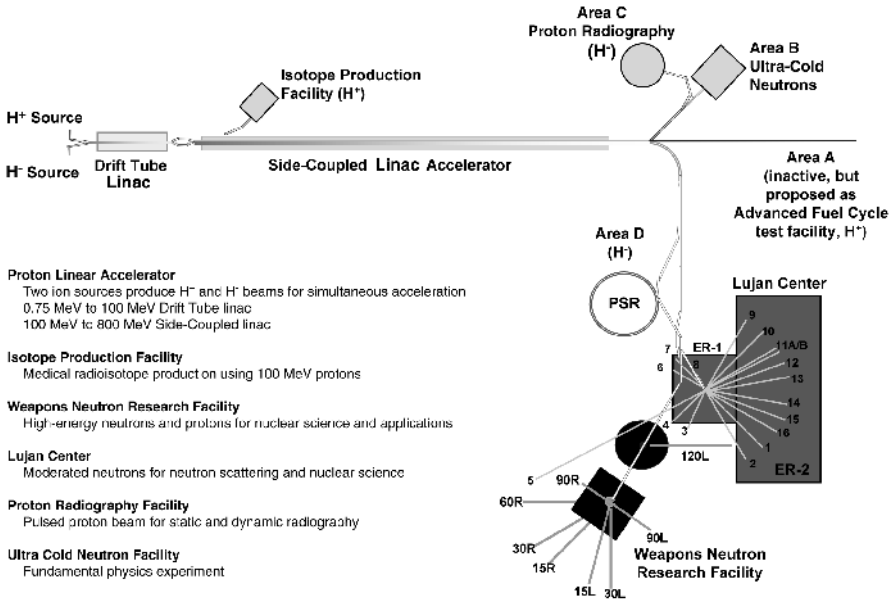

Figure 9. Layout of the LANSCE user facility (Lisowski 2005).

the proton current is virtually unlimited and, hence, the neutron flux can be, in principle, increased without a physical limit. At reactor sources, this is not possible due to reactor safety. Furthermore, spallation neutron sources are, due to the time structure of the neutron flux, ideal for time-of-flight (TOF) measurements. The projected Spallation Neutron Source (SNS) at Oak Ridge National Laboratory, U.S.A., (Fig. 10) is designed for proton currents of 2 mA at 1 GeV proton energy on a liquid mercury target at a repetition rate of 60 Hz, resulting in a peak neutron flux on the order of 10^{17} neutrons cm^{-2} s^{-1} (Mansur et al. 2001; Mason et al. 2002, 2005). The spallation neutron source KENS (Ikeda 2002) under construction at Tokai, Japan, is designed for a 333 μA current of 3 GeV protons, also with a liquid mercury target and generating a peak neutron flux on the order of 10^{17} neutrons cm^{-2} s^{-1}. The U.S. and Japanese spallation neutron sources are scheduled to become available in 2007. The ESS (European Spallation Source, Richter 2002) was designed to a similar flux (ESS 2003), but the project was canceled in 2003 by European authorities.

Other neutron sources

Another way to generate neutron bursts are pulsed reactors: Two neutron reflectors are rotated with fissile material in-between, such that a short chain reaction is induced when both reflectors are in appropriate orientation, generating a neutron pulse. The research reactor IBR-2 at Dubna, Russia, operates according to this principle and generates neutron pulses of 320 μs half-width at 5 Hz with a peak neutron flux of 5×10^{15} neutrons cm^{-2} s^{-1} (JINR 2005). The Swiss spallation neutron source SINQ generates a continuous current of spallation neutrons from a 590 MeV continuous proton beam running at 1.8 mA (i.e., without a storage ring to accumulate the protons to intense bursts), resembling a medium flux research reactor (PSI 2002). The time averaged flux emitted from the moderator is 1.6×10^{13} neutrons cm^{-2} s^{-1}.

Compact, portable neutron sources utilize spontaneous fission, α-emitters or nuclear fusion for neutron generation. Spontaneous fission occurs for instance in the isotope ^{252}Cf,

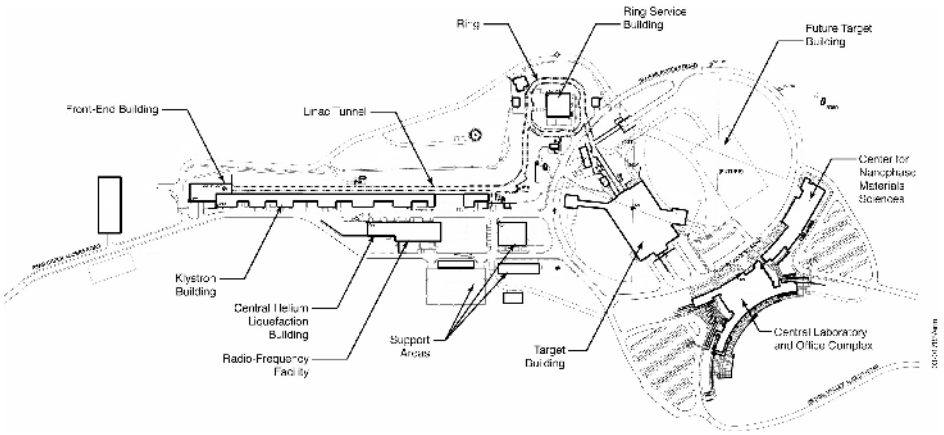

Figure 10. Layout of the Spallation Neutron Source (SNS) in Oak Ridge, Tennessee, U.S.A. (courtesy of Oak Ridge National Laboratory).

which has to be produced from uranium or other transuranic elements by successive neutron capture processes in a nuclear reactor. One milligram of ^{252}Cf produces 2.3×10^9 neutrons s^{-1}. A fresh commercial ^{252}Cf source typically produces of the order of 10^8 neutrons s^{-1}, but ^{252}Cf has a half-life of 2.6 years, resulting in a source intensity decrease to half of its initial intensity over 2.6 years. Neutron generation using α-emitters (Pu, Am, Ra) is based on mixed powders of an isotope decaying by emission of α-particles and a light element, typically Beryllium. The emitted α-particle may generate a neutron based on the nuclear reaction

$$^{9}\mathrm{Be} + \alpha \rightarrow {}^{12}\mathrm{C} + \mathrm{n} \tag{5}$$

Such sources also produce neutron intensities of 10^8 neutrons s^{-1}. These two types of neutron generators are called isotopic neutron sources and have the disadvantage that they cannot be pulsed or turned off, requiring bulky shielding at all times. Their energy spectrum is broad and the intensities are too low for scattering applications, but they may be used for element identification using neutron activation analysis, simple radiography applications or for detector calibration, development and testing.

Tabletop neutron generators based on nuclear fusion have evolved from large, expensive instruments to compact and affordable devices. These sources utilize deuterium (^{2}H, D) or tritium (^{3}H, T) nuclear fusion reactions to produce neutrons:

$$\mathrm{D} + \mathrm{T} \rightarrow {}^{4}\mathrm{He} + \mathrm{n} \tag{6}$$

$$\mathrm{D} + \mathrm{D} \rightarrow {}^{3}\mathrm{He} + \mathrm{n} \tag{7}$$

For the nuclear fusion process, deuterium ions are produced from a metal-hydride based deuterium source, accelerated and steered into a deuterium or tritium target, also made out of a metal hydride containing deuterium or tritium. Since these sources are accelerator based, the neutrons can be produced in pulses and the source can be switched off. Typical neutron intensities are of the order of 10^9 neutrons s^{-1}, but neutron generators with intensities up to 10^{13} neutrons s^{-1} are under development (Reijonen et al. 2005), making such generators potentially interesting for neutron scattering applications in the future. Portable neutron generators are also useful for applications in the field, for instance for the determination of soil humidity (Pouzo et al. 2003) or the detection of drugs and explosives (Womble et al. 2001).

BEAM CONDITIONING

Neutron moderation

Both at steady-state (reactor sources) and pulsed sources, the generated neutrons initially have energies far too high to be suitable to measure properties relevant to solid state physics. Particle kinetic energy E and wavelength λ are related by de Broglie's law:

$$E = \frac{p^2}{2m} = \frac{(\hbar k)^2}{2m} = \frac{h^2}{2m\lambda^2} \tag{8}$$

where p is the particle's momentum, m its mass, $\hbar$ is Planck's constant h over 2π, and $k = 2\pi/\lambda$ is the wave-vector of the particle. For measurements of the static distribution of the atoms in a solid (e.g., the crystal structure in crystalline or the average atomic distances in amorphous solids), the wavelength must be of the order of the interatomic distance, equivalent to energies of several tens of meV in the case of neutrons (for X-rays, this energy is in the range of several tens of keV). Measuring the dynamic distribution of atoms (i.e., measurements involving phonons) requires neutron energies of the same order of magnitude. Therefore, the neutron energy must be reduced from the order of 2 MeV and 100 MeV for reactor and spallation neutrons, respectively, to the order of 10 meV. The kinetic energy of neutrons can only be changed by collisions with nuclei as neutrons have no charge. By guiding the neutron beam through appropriate materials like water, hydrogen or methane, the neutrons lose energy in collisions with atoms and molecules. This process is called moderation. In thermal equilibrium with the moderator medium, the neutron energies are of the order of magnitude of thermal vibrations of the moderator atoms, and thus the neutrons may gain as well as lose energy. The mean energy of the neutron spectrum after the moderation process is given by

$$E = \tfrac{3}{2} k_B T \tag{9}$$

(k_B is Boltzmann's constant, T the moderator temperature), resulting in an intensity maximum slightly lower than this energy, since the so-called Maxwellian energy distribution of neutrons leaving the moderator is slightly asymmetric. Neutrons with energies corresponding to room temperature are called thermal neutrons. As such, the moderation process in this case is called thermalization. As Bacon (1955, sect. 1.2) states, it is just a 'fortunate circumstance' that these wavelengths and energies are those energies desired for investigations of atomic arrangements and phonon energies in solids, making the moderation process relatively convenient. It is remarkable that a water layer of only 2.5 cm is sufficient to decrease the neutron energy by 10 orders of magnitude. Figure 11 shows examples of neutron flux emerging from moderators at

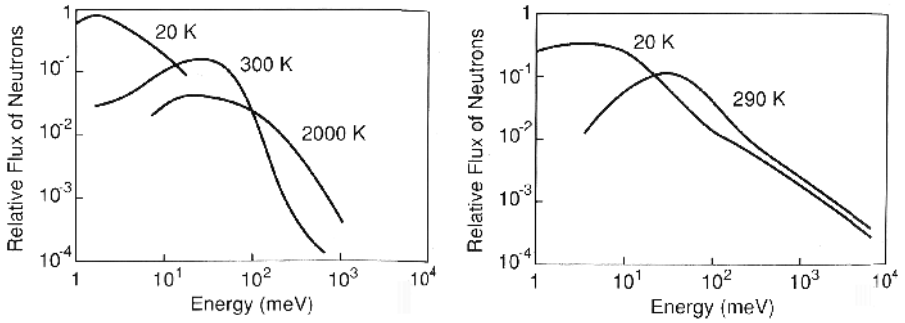

Figure 11. Relative neutron flux as a function of energy for the high-flux reactor at the ILL for different moderator temperatures (*left*). Similar spectra from the spallation source LANSCE (*right*) (Pynn 1990).

different temperatures at the reactor of the ILL and the LANSCE spallation source. The 'hot' source at ILL, with a moderator temperature of 2000 K, consists of radiation heated graphite and is the only one of its kind in the world.

The velocities of thermal neutrons are on the order of 1000 m/s. Thus, relativistic effects can be neglected. The moderation process introduces a broadening of the initially sharp neutron pulse at a spallation source (e.g., ~270 ns initial neutron pulse width at LANSCE, determined by the pulse width of the proton pulse), which can be, for example, approximated for the water moderator used at the HIPPO instrument at LANSCE by

$$\Delta t = \frac{7.1}{\sqrt{E}} \approx 25\lambda \tag{10}$$

where Δt is the halfwidth in μs of a neutron pulse of wavelength λ (given in Å), and energy E (given in eV). Therefore, the pulse widths are, for instance, 7, 32, and 225 μs for neutron energies of 1 ($\lambda = 0.3$°Å), 0.05 (1.3 Å), and 0.001 eV (9 Å), respectively. Converted to d-spacing resolution $\Delta d/d$, the above figures result in an instrumental contribution to reflection broadening from the moderator of 1.7×10^{-3}. With a 25 mm thick water moderator, both high intensity and high resolution (i.e., small instrumental broadening) moderators can be built by placing a gadolinium foil (e.g., 0.38 mm thick for LANSCE water moderators) either 8 mm or 18 mm away from the spallation target within the water (Windsor 1981, section 3.4). Gadolinium is a strong neutron absorber and the absorption cross-section is proportional to the neutron velocity, hence thermalized, slow neutrons are more likely to be absorbed than still un-moderated fast neutrons. The neutron pulse width or instrument resolution is determined by the distance the already thermalized neutrons travel in the moderator before leaving the moderator towards the sample. Therefore, in the first case the relatively small amount of neutrons already thermalized in the first 8 mm within the moderator is very likely absorbed by the gadolinium while the un-moderated, fast neutrons pass the foil to become moderated in the larger downstream section of the moderator. This results in a relatively high flux at the cost of a relatively large instrumental contribution of the moderator to the width of Bragg-reflections (i.e., poorer resolution). In the second case the gadolinium absorbs the large amount of neutrons thermalized in the larger section towards the source, while the smaller number of neutrons moderated in the 7 mm thick layer towards the sample provides a smaller contribution to the instrumental resolution, resulting in sharper reflection peaks at the cost of a lower neutron flux.

The neutron intensity in an experiment using polychromatic neutrons varies as a function of neutron energy (or wavelength, see Fig. 11). The spectrum of the incident neutrons for a given instrument is required, for instance, to normalize diffraction spectra to allow the comparison of peak intensities. This spectrum can be measured using a "zero scatterer," such as vanadium. A zero scatterer does not produce a coherent diffraction pattern, i.e., no Bragg diffraction peaks occur. The incoherent scattering from the material results in a detected spectrum proportional to the incident neutron intensity. After moderation, the neutron spectrum at a spallation source is an overlay of $1/E$ (Eqn. 3) and Maxwellian (Eqn. 4) distributions, Figure 11. The effect of the normalization on the diffraction pattern of silicon is shown in Figure 12, where the raw diffraction data measured for a silicon powder sample (Fig. 12a) is divided by the incident intensity (Fig. 12b) to produce a normalized diffraction pattern that is used for subsequent analysis (Fig. 12c).

Choppers and filters

Neutron beams emerging from a moderator may require some conditioning for a given application. *Beam choppers* are devices with either a neutron absorbing or highly scattering rotating disk containing one or more openings, or a two-armed rotor (chopper blade) made of neutron absorbing material. In the first case, a constant, typically polychromatic beam is broken up into short pulses, allowing measurement of the energy of a neutron by its time-of-flight for the known distance between sources and the detector. Choppers of the second kind

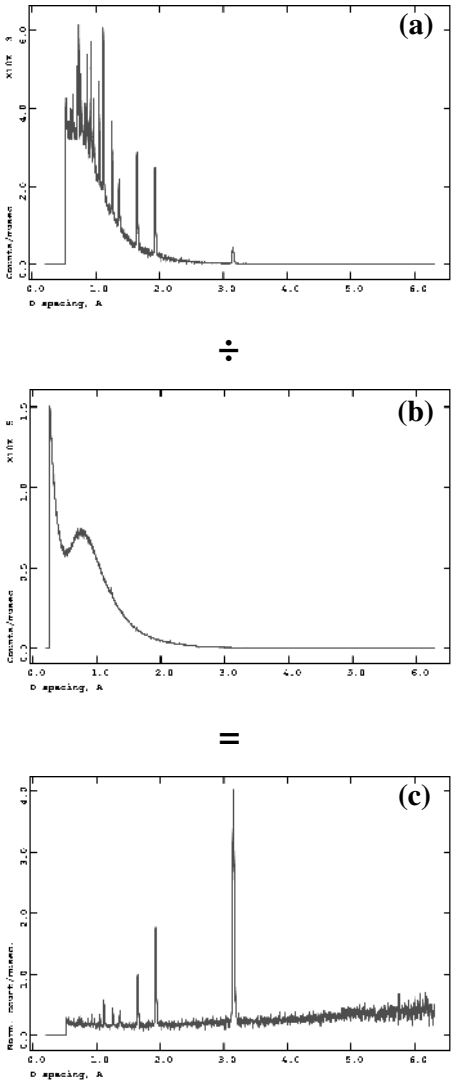

Figure 12. (a) A diffraction pattern measured at a pulsed spallation source (the example shows silicon powder) needs to be normalized by the incident intensity (b) to correct for the wavelength-dependence of the incident intensity (c). The conversion from time-of-flight to *d*-spacing is performed for the 90º detector bank of the HIPPO instrument to illustrate the neutron intensity available over the *d*-spacing range of this detector bank.

are called T_0-choppers and used to block high energy neutrons and gamma radiation originating from the spallation process at a spallation neutron source, which would cause severe background or damage to the sample otherwise. They also prevent fast neutrons from arriving at a detector together with slow neutrons from the previous pulse. Figure 13 illustrates this so-called frame overlap: The neutrons in each moderated pulse at a pulsed source begin their flight to the detector at essentially the same time (within a small fraction of a millisecond). However, because they all have different energies (velocities), as time passes they spread out, reaching the same distance from the moderator at different times after departure. That situation is depicted graphically in Figure 13 in plots of distance traveled versus time for neutrons with various energies. Each "explosion" on the time axis represents a pulse of neutrons emerging from the moderator. Note that fast neutrons from, say, the second pulse can reach a detector 12 m distant at the same time as slow neutrons from the first pulse. To prevent such "frame overlap", which interferes with time-of-flight measurements, a spectrometer can be equipped with a frame-overlap chopper. Because of the two rotor blades, the chopper is rotated at half the repetition rate of the neutron pulses (for instance, 10 times per second at LANSCE with a 20 Hz neutron pulse frequency, Fig. 14) and at a certain phase relative to the proton pulse, it blocks neutrons with energies corresponding to wavelengths less than 16 Å. That mode of chopper operation is represented in Figure 13 by a thick horizontal line at a distance of 6.25 m. Changing the phase of the chopper by 90° (moving the thick horizontal line to the left or right a distance equal to its length) blocks neutrons with energies corresponding to the wavelengths between 16 and 32 Å. Figure 14 shows a combination of a T_0-chopper and a frame overlap chopper. The former blocks by scattering and absorption the burst of high-energy neutrons and gamma rays (light grey in Fig. 14) that precedes the pulse of moderated neutrons; the latter absorbs lower-energy neutrons that would cause frame overlap as they spread out along the flight path because of their different energies (Fig. 13). In Figure 14, by t = 10 μs the T_0-chopper, which rotates 360° every 50 ms, has eliminated the flash of γ radiation from the spallation and scattered neutrons with energies down to 0.91 MeV.

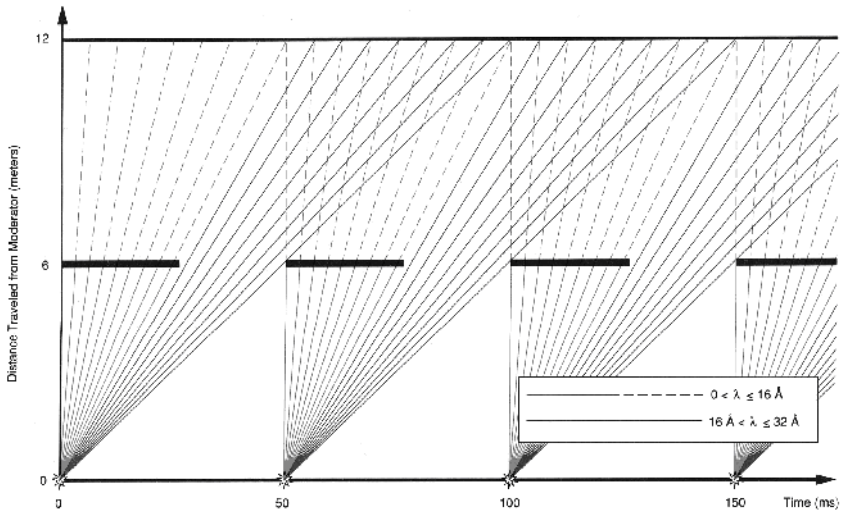

Figure 13. The frame overlap problem at a pulsed source (Hyer and Pynn 1990).

By t = 15 ms the T_0-chopper has removed neutrons down to 300 meV and rotated out of the beam. Energetic thermal neutrons (around a wavelength of 1 Å, light to dark grey in Fig. 14) have reached the frame-overlap chopper, which rotates 180° every 50 ms, and are removed. The remaining neutrons in the pulse have spread out along the flight path. By t = 40 ms the frame-overlap chopper has absorbed neutrons down to 0.3 meV (dark grey) and rotated out of the beam, allowing very slow neutrons (black to white) to proceed on to the sample. By changing the phase of the frame-overlap chopper, faster neutrons, rather than slower neutrons, can be allowed to reach the sample. Obviously, such choppers have to be carefully synchronized with the neutron source frequency.

A third type of chopper allows extraction of neutrons within a defined energy band from a "white" (polychromatic) neutron beam as illustrated in Figure 15. A neutron (dot) traveling from left to right can, if it has the proper energy (velocity), pass through the center of a curved slit in a rotating disk. Shown in Figure 15 are four snapshots of the neutron making its passage through one of several slits in an energy defining chopper. To an observer moving with the neutron, the slit appears to open up in front of the neutron. Neutrons that do not have the proper velocities strike the walls of the slits and are absorbed. A chopper of this type can be used to select a narrow band of neutron energies from either the incident or the scattered beam. Different neutron energies with a rather broad spectral resolution can be selected by changing the speed of the chopper rotation. Hence, these choppers are also termed "selectors."

Some applications require neutrons to have wavelengths greater than a certain critical wavelength. This can be achieved using a *neutron filter*: in a polycrystalline material, all crystal orientations will be present and all available lattice planes will reflect neutrons away from the incident beam direction. For a sufficiently thick sample, this results in a complete attenuation of all neutrons of wavelengths fulfilling Bragg's law. Only neutrons of wavelengths greater than $2d_{max}$ are transmitted through the sample and, thus, the material acts as a neutron filter.

Neutron transport and neutron optics

Neutrons are neutral particles and hence cannot be steered by electromagnetic fields like protons or electrons. The neutron flux is reduced proportional to the square of the distance L

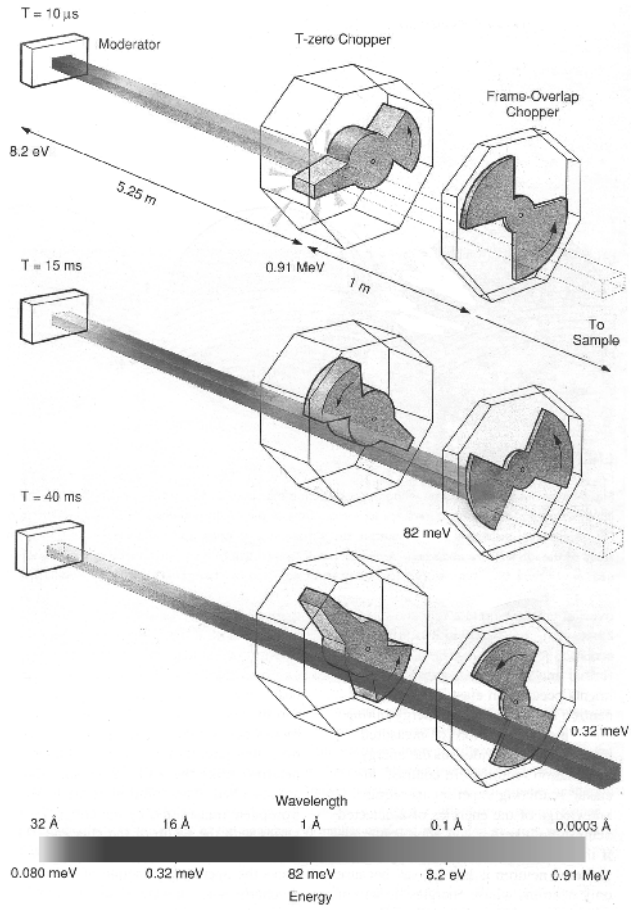

Figure 14. Schematic of a T_0-chopper and a frame-overlap chopper (Hyer and Pynn 1990).

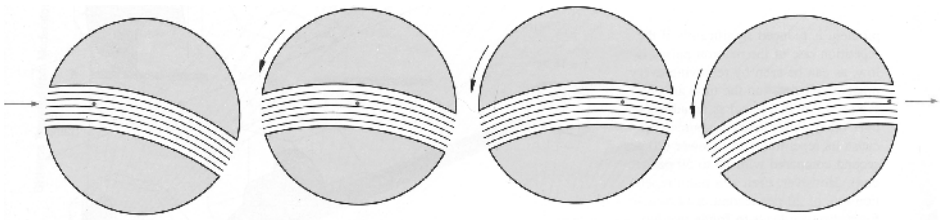

Figure 15. Schematic of an energy defining chopper that can be used as a monochromator (Hyer and Pynn 1990).

from the source since it is proportional to the solid angle Ω covered by the beam spot size *A*

$$\Omega = \frac{A}{L^2} \tag{11}$$

For example, at the HIPPO beam line at LANSCE, the initial flight path length is 9 m and a typical beam spot size is 10 mm diameter, resulting in a covered solid angle of $\Omega = 79\ \text{mm}^2/81\ \text{m}^2 \approx 10^{-6}$ sr (steradian, this solid angle corresponds to $\sim 8\times10^{-6}\%$ of 4π). Additional losses of the neutron intensity caused by absorption and scattering in air can be avoided by using evacuated beam or drift tubes. Without the evacuation, the beam intensity is reduced by ~5% per meter in dry air. The losses can be further reduced by neutron guides or super-mirrors, which utilize the effect of total reflection, well-known from the optics of light.

Along total-reflecting surfaces, like thin Ni (or even more efficiently ^{58}Ni) layers deposited on glass, neutrons can be guided from the source to the instrument with almost no loss. It has already been shown by Fermi and Marshall (1947), that if the *coherent scattering length*, b_{coh}, is positive, a refractive index, n, for neutron waves can be derived:

$$n = 1 - \frac{\lambda^2}{2\pi} \cdot N \cdot b_{coh} \tag{12}$$

where N is the number of identical nuclei of scattering length b_{coh} per cm^3. Thus, most materials are neutron-optically less dense ($n < 1$) than air or vacuum. Therefore, neutrons incident on the surface of such media are totally reflected almost without loss as long as their angle of incidence is below the critical angle, ε, defined by

$$\varepsilon = \lambda \sqrt{\frac{N \cdot b_{coh}}{\pi}} = \lambda_c \cdot \sqrt{\frac{N}{\pi}} \sqrt[4]{\frac{\sigma_{tot}}{4\pi}} \tag{13}$$

where σ_{tot} is the total coherent scattering cross section. For a given angle of incidence $\alpha \le \varepsilon$, total reflection can only occur if the neutron wavelength is greater than the critical wavelength λ_c. Typical critical wavelengths are ~1 Å, meaning that reflection is most efficient for slow neutrons, which have low intensities at reactor and spallation sources. A neutron guide can be given a slight curvature, so that only slow neutrons, which fulfill the condition of total reflection, will follow the bent guide, while fast neutron and gamma ray backgrounds will end up in the absorber material surrounding the guide. The principle of total reflection can also be utilized for polycapillary focusing optics, where neutrons are guided through bend channels of diameters on the order of micrometers. Such polycapillary focusing optics typically consist of a fused bundle of tapered polycapillary glass fibers. Figure 16 shows a schematic of such a device, converging a uniform parallel beam into a point by multiple glancing-angle deflections from the inside walls of the channels (upper part of Fig. 16). Beam spot sizes of ~500 μm with a flux gain of the order of 100 compared to the divergent beam on the same area are achievable with this technique (Xiao et al. 1994), which also can be used to bend cold neutron beams by up to 20° (Chen et al. 1992). Neutron lenses are also feasible, with converging neutron lenses being concave rather than convex as for light since the refractive index is smaller than 1. With neutron lenses, flux gains of the order of 10 are possible (Eskildsen et al. 1998).

Since neutrons have a spin and a magnetic moment, μ_n, an interesting phenomenon arises from the reflection on magnetized mirrors. In this case the index of refraction depends also on the relative orientation of the direction of magnetization and the neutron spin:

$$n_{\pm} = 1 - \frac{\lambda^2}{2\pi} \cdot N \cdot \mp \frac{\mu_n \cdot B}{2 \cdot E_n} \tag{14}$$

where ∓ refers to the orientation of the magnetic field B with respect to the neutron spin, and

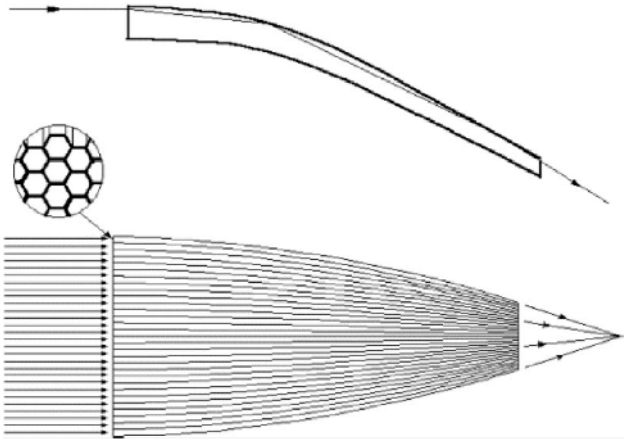

Figure 16. Schematic of a poly-capillary monolithic focusing optic. The inset illustrates the individual hexagonal close-packed channels (Gibson et al. 2002).

E_n is the neutron energy. As can be seen from this equation, neutrons with the same energy or wavelength, but opposite spin orientations have different critical angles. As such, magnetized mirrors can provide a method to polarize neutrons, if suitable materials are chosen.

Neutron super mirrors may also be used to focus neutron beams into small cross sections (Goncharenko et al. 1997, 2003). High intensity in small beam spots through focusing are of particular interest for high pressure experiments, small single crystals, or position sensitive strain scanning. The Kirkpatrick-Baez setup, originally developed for synchrotron radiation, was successfully demonstrated for neutrons by Ice and coworkers (Ice et al. 2005) who achieved a neutron spot-size of 100 μm with a flux gain of 37 compared to the divergent beam of the same cross section. In the Kirkpatrick-Baez mirror setup, beam divergences in the horizontal and vertical beam planes are focused sequentially by crossed mirrors that each focus in their plane of reflection (Fig. 17, see also Fig. 13 in Parise 2006, this volume). It can be expected that this concept will become more routinely available at neutron sources in the future. As all techniques relying on total reflection, neutron super-mirror based neutron optics work best for neutrons with wavelengths greater than ~1 Å.

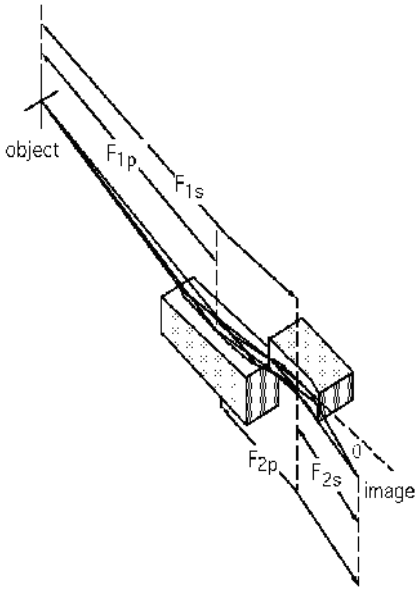

Figure 17. Kirkpatrick-Baez mirror pair. Elliptical mirrors focus from one focus to another in the plane of reflection. The rays act almost independently in the vertical and horizontal focusing planes (Ice et al. 2005).

The actual beam spot size for scattering experiments is typically defined through movable slits ("jaws"), pin-holes or cylinders made out of neutron absorbing materials. A pair of slits, a distance L apart, provides a rudimentary collimator with a defined beam divergence of

$$\alpha_{\max} = \frac{a_1 + a_2}{L} \tag{15}$$

where a_1 and a_2 are the widths or diameters of the slits or pinholes. Elements that have a large absorption cross-section for thermal neutrons in their natural isotope mix are boron, cadmium and gadolinium. Boron-carbide and boron-nitride are materials commonly used for collimators, whereas cadmium metal and gadolinium-oxide based paint are used for experiment-specific masking of sample environments. Fast neutrons still penetrate these materials, hence, if background due to fast neutrons needs to be reduced, T_0 choppers as described above are the preferred method. Similar to X-ray instruments, secondary collimation is used to reduce background originating from air scatter or interaction of the primary beam with the sample environment. Such collimators are typically comprised of mylar blades coated with gadolinium oxide paint. To avoid blind spots and achieve homogeneous transmission through the collimator, radial collimators are generally oscillated or continuously rotated (Wright et al. 1981). The collimators may also be used in a stationary mode to define a diffraction volume buried inside the volume of a larger sample to allow spatially resolved measurements, for instance to measure gradients in phase composition or strain as a function of depth (Withers et al. 2000). Achievable volumes at current sources for this technique are of the order of cubic millimeters, but can be expected to get smaller with neutron focusing improvements and more powerful neutron sources. Figure 18 shows the principle layout of a neutron strain scanner at a reactor source, utilizing neutron guides, collimators, and apertures.

NEUTRON INSTRUMENTS

Diffraction with constant wavelength methods

The neutron wavelengths or energy can be determined before and after interacting with the sample by scattering neutrons off a single crystal or a polycrystal with highly oriented grains of known lattice parameters. In a *constant wavelength* (CW) experiment, utilizing Bragg's law

$$\lambda = 2d \sin\theta \tag{16}$$

the wavelength can be selected from the Bragg-angle θ and the known lattice spacing d of the reflecting set of lattice planes (monochromator). This process is used at reactor sources and

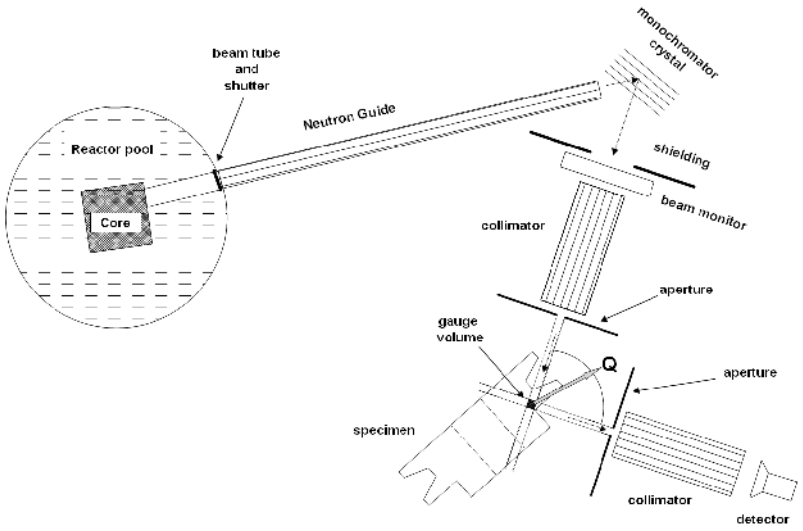

Figure 18. Layout of a neutron strain scanner at a reactor source.

requires large beam windows in sample environments, large collimators and large position sensitive detectors or is time consuming if many different angles have to be probed by a moving detector in order to get an intensity versus diffraction angle ($I(\theta)$) histogram. The principle is very similar to a constant wavelength experiment with X-rays.

Diffraction experiments with monochromatic radiation can be done on single crystals, powders or polycrystals and there is a large variety of instruments. Some use point detectors and reciprocal space is scanned by rotating the sample on a goniometer as well as varying the Bragg angle. Other instruments use 2D position sensitive detectors and a large 2θ range can be recorded simultaneously. Instruments such as D1B, D2B (Fig. 18 in Redfern 2006, this volume) and D20, all at ILL, are of this type and are particularly useful to analyze time-dependent processes such as chemical reactions as function of temperature or to investigate textures (Bunge et al. 1982). The D20 instrument is described in detail in Kuhs and Hansen (2006, this volume; see their Figs. 1 and 2). There are diffractometers with 2D position sensitive detectors, such as D19 at ILL with a detector aperture of 4° by 64° and a *d*-spacing range of 0.5 to 100 Å, which is mainly used for single crystal studies of small samples with large unit cells (Detti et al. 2004). Another single crystal diffractometer is the Very-Intense, Vertical-Axis Laue DIffractometer VIVALDI, also at the ILL (Fig. 1 in Ross and Hoffman 2006, this volume). It utilizes a polychromatic neutron beam and a neutron-sensitive image plate detector to record Laue patterns of stationary single crystals. VIVALDI has been applied to problems such as crystal structure solution of large organic crystals, magnetic structures or high pressure research (McIntyre et al. 2005).

Diffraction with Time-of-Flight (TOF) methods

The second method to determine diffraction patterns uses pulsed neutrons and determines the time, *t*, it takes for a neutron to travel a given distance, *L*. This can be achieved by generating neutron pulses, either by chopping a steady neutron current from a reactor or generating the neutrons in pulses. The latter is found at most spallation sources (with the PSI in Switzerland being the exception) and hence the TOF-method is the method of choice at such facilities. By equating the quantum mechanical momentum (de Broglie-relation) and the classical mechanics momentum, one derives

$$p_{QM} = \hbar k = mv = p_{CM} \leftrightarrow \frac{h}{\lambda} = m\frac{L}{t} \leftrightarrow \lambda = \frac{ht}{mL} \tag{17}$$

With Bragg's law, this becomes

$$\lambda = 2d\sin\theta = \frac{ht}{mL} \leftrightarrow d = \frac{h}{\underbrace{2mL\sin\theta}_{\text{const}}} \cdot t \tag{18}$$

Hence, using the time-of-flight technique, the d-spacing is directly proportional to the measured time-of-flight, with all other parameters being constant. Compared to a constant wavelength experiment, the most important difference is that any given detector records the full diffraction pattern $I(t)$ (energy-dispersive) with each neutron pulse for its unique scattering vector such as shown in Figure 12. To improve counting statistics, multiple pulses are summed up and multiple detectors are typically integrated after appropriate corrections for differences in L and θ. The constant Bragg angle allows for smaller beam windows and stationary detectors, simplifying design of sample environments.

Also at pulsed sources there are instruments specialized for single crystals such as SCD at IPNS and LANSCE with 2D position sensitive detectors (Fig. 3 in Ross and Hoffman 2006, this volume) and the instrument TOPAZ under construction at SNS (Fig. 11 in Ross and Hoffman 2006, this volume). Most powder diffractometers have multiple detectors for more efficient counting. Examples are GEM and POLARIS (Fig. 10 in Redfern 2006, this volume) and

ENGIN-X (Fig. 3c in Daymond 2006, this volume) at ISIS, GPPD at IPNS, SKAT at Dubna (Fig. 9 in Wenk 2006, this volume) and NPDF (Fig. 4 in Proffen 2006, this volume), HIPD, SMARTS and HIPPO at LANSCE. Depending on the application, some of these instruments are optimized for resolution (such as residual strain measurements), intensity (e.g., to record time-dependent processes), angular range (such as small angle neutron scattering, SANS; see Radlinski 2006, this volume) or texture (with detectors in different positions recording differently oriented crystals (Wenk 2006, this volume). The layout of the time-of-flight powder diffractometer HIPPO (which stands for High Pressure - Preferred Orientation) at LANSCE (Wenk et al. 2003; Vogel et al. 2004) is shown in Figure 19. It is unique in having a total of 1360 ^{3}He detector tubes distributed over 50 detector panels arranged on 5 banks at different Bragg angles of 140°, 90°, 40°, 20°, and 10°. The large sample chamber can accommodate a wide range of ancillary equipment such as an automatic sample changer, a load frame, various high pressure cells, cryostats, furnaces, as well as user supplied equipment.

It is worth noting that all lattice planes reflecting into a given detector in a TOF experiment share the same normal direction. This fact can be used for instance in an *in situ* deformation experiment to probe responses of various lattice planes *hkl* (in different grains) in the same direction relative to the applied load (Daymond 2006, this volume). In a constant wavelength experiment each probed lattice plane has a different direction relative to the applied load unless the sample is rotated appropriately.

d-spacing resolution

For constant wavelength as well as pulsed neutron beams, the instrument resolution can be derived from Bragg's law by calculating the propagated uncertainty:

$$d = \frac{\lambda}{2\sin\theta} \Rightarrow \frac{\Delta d}{d} = \sqrt{\left(\frac{\Delta\lambda}{\lambda}\right)^2 + \left(\Delta\theta\cot\theta\right)^2} \tag{19}$$

This means that the sharpest peaks appear in back-scattering geometry ($2\theta > 90°$). For a TOF experiment, the wavelength is proportional to the TOF, and hence $\Delta d/d$ has a contribution from

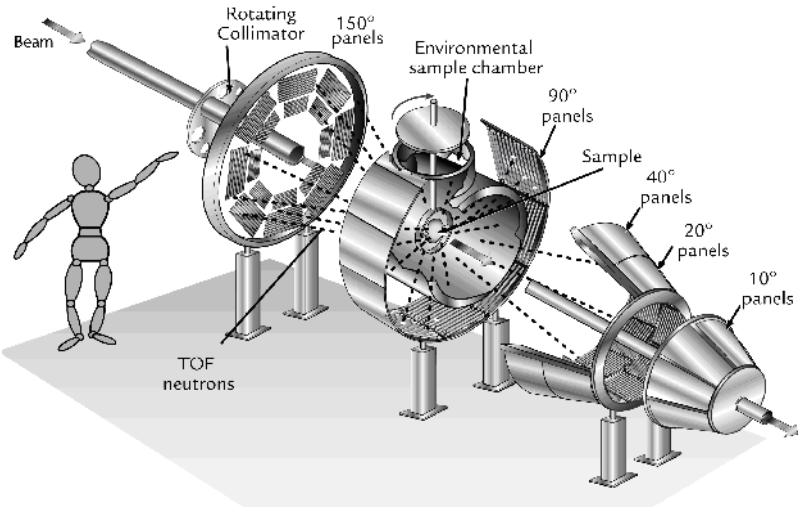

Figure 19. Schematic of the neutron time-of-flight powder diffractometer HIPPO at LANSCE. The detector tubes are arranged on 50 detector panels on 5 rings. The distance between the 150° and the 10° banks is ~3 m (Wenk et al. 2003).

$\Delta t/t$. The time uncertainty in a pulsed experiment is typically determined by the moderation time, which is wavelength dependent, and the bin width of the detector electronics. As shown in Equation (17), the wavelength in a pulsed neutron beam experiment is also proportional to $1/L$, resulting in a contribution of $\Delta L/L$ to the instrument resolution. The main contributions to the flight-path uncertainty are moderator thickness and divergence. This means that peaks get sharper with increasing flight-path length, resulting in a trade-off between resolution and flux, which decreases with $1/L^2$, in the design of an instrument (Johnson and Daymond 2002). Figure 20 shows a section of the diffraction pattern of CaF_2 measured on three detector banks with different diffraction angles on the HIPPO (9 m flight-path from moderator to sample) and SMARTS (31 m flight-path from moderator to sample) instruments at LANSCE. The variation in resolution with the diffraction angle (HIPPO detectors) and flight path length (HIPPO 90° and SMARTS 90° detectors) is evident in the peak broadening. For comparison, the same material was measured with a conventional laboratory X-ray source (Rigaku Ultima III, 2 hours data collection, divergent beam of 0.6° between source and detector, 0.6 mm detector slit, graphite monochromator in front of detector). The resolution of the X-ray powder diffractometer is sufficient to resolve the K_α/K_β splitting of the peaks, a much better resolution than even the relatively good resolution of the SMARTS neutron diffractometer. Also, the differences in the structure factors for the two types of radiation are evident, resulting in some peaks becoming almost extinct with X-rays.

Nuclear Resonance Spectroscopy

The time-of-flight method not only allows resolving the wavelength of scattered neutrons, but also the $I(E)$ spectrum of the transmitted neutrons. For a transmission experiment, the detector is located in the direct beam behind the sample ($2\theta = 0°$)[1]. This facilitates the utilization of nuclear resonance spectroscopy for temperature measurements: Certain isotopes have sharp and well defined absorption resonances, i.e., only neutrons (typically epithermal) of a well defined energy are absorbed. A change in temperature increases the thermal motion of the nuclei and causes a Doppler broadening of the resonance spectrum. By fitting appropriate resonance profiles to the measured data, the broadening can be accurately determined and, after calibration, the sample temperature can be measured to ±10 K without thermocouples or optical access to the sample for pyrometry. Thin foils of resonant material in the hot zone of a furnace or temperature/pressure cell allow temperature measurements without major additional diffraction peaks (Stone et al. 2005a,b). Figure 21 shows an example of nuclear resonance spectra of hafnium at three different temperatures. Note that the resonance width does not change with pressure, hence, the observed change in width is due to the change in temperature only.

Inelastic scattering

The energy of thermal neutrons is comparable to the energy of lattice phonons and molecular vibrations, resulting in *inelastic neutron scattering* during which a neutron can gain or lose energy due to interaction with a phonon or vibrational modes of a molecule (Loong 2006, this volume). The triple axis spectrometer (TAS), found at most research reactors, is the most versatile instrument for single crystal spectroscopic measurements. Figure 22 shows a schematic of the cold neutron three-axis spectrometer IN12 at ILL as an example of this type of instrument. Similar instruments are IN14 at ILL and T2 at LLB. Utilizing Bragg diffraction, a monochromator defines the wave vector (i.e., direction and energy/wavelength) of the incident neutrons, $\mathbf{k_i}$. After interaction with the sample, Bragg reflection by an analyzer crystal

[1] The term "transmission" is also used in "transmission diffraction," describing a diffraction geometry where the diffracted beam exits the sample volume on the opposite side of the incident beam. In this case, neutrons which were scattered by the sample are measured, whereas in a true transmission experiment those neutrons are measured which did not interact with the sample.

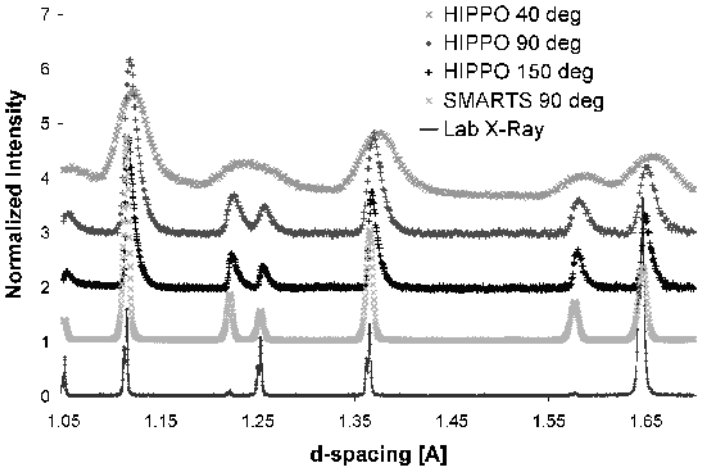

Figure 20. Section of the diffraction pattern of CaF_2 measured on the HIPPO (different detector banks) and SMARTS neutron diffractometers at LANSCE and with a conventional X-ray source.

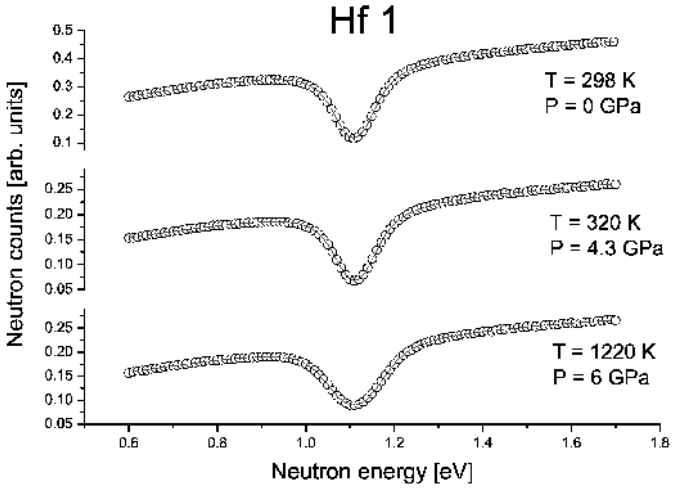

Figure 21. Nuclear resonance spectra of hafnium as a function of temperature (pressure changes do not affect the resonance shape, courtesy of B. Winkler).

determines the wave vector after scattering, $\mathbf{k_f}$. From these two, the momentum transfer

$$\mathbf{Q} = \mathbf{k_i} - \mathbf{k_f} \tag{20}$$

and the energy transfer, ω, from neutron to sample or vice versa can be determined. Phonon dispersion curves can be measured using this technique, even with samples at non ambient conditions in a furnace, cryostat, or pressure cell. Inelastic neutron scattering is particularly powerful in combination with molecular dynamics simulations (Trouw 1992; Johnson et al. 2000). Instruments to measure phonon dispersion curves also exist at pulsed sources, where choppers are used to select the wavelength of the incident neutrons. Vibrational spectra are obtained by neutron energy loss during scattering from the sample as incoming neutrons excite

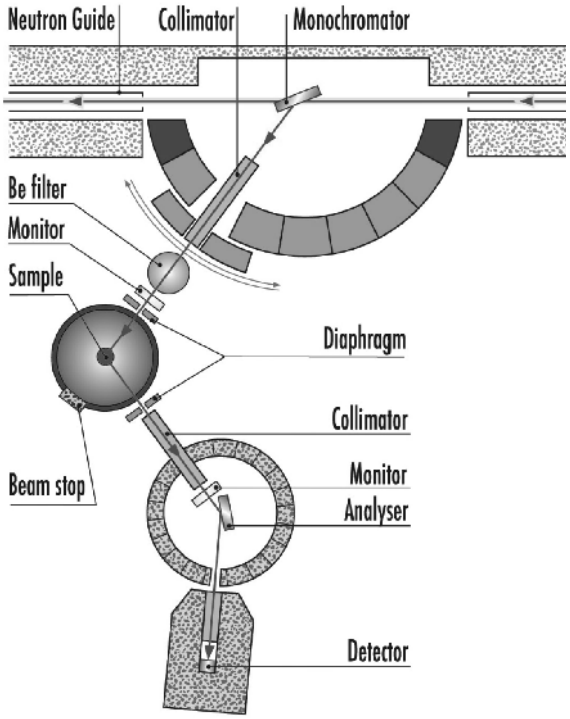

Figure 22. Schematic of the cold neutron triple axis spectrometer IN12 at the ILL (Schmidt and Raymond 2005).

molecular vibrations by giving up energy (Kearley 1995; Mitchell et al. 2005). Typical results from such experiments are interatomic force constants and estimates of bond strengths, in particular for bonds involving hydrogen. Instruments for this type of measurement exist both at pulsed sources and reactor sources, e.g., QENS at IPNS (Fig. 6 in Loong 2006, this volume).

Neutron radiography

The first study using neutron radiography was made by Kallmann and Kuhn in the 1930's in Germany (Kallmann 1948), but only after the pioneering work of Harold Berger (Berger 1965), did neutron radiography become widely accepted as a two-dimensional imaging method for use in non-destructive testing. Today most research reactors are equipped with radiographic facilities (Winkler 2006, this volume). Radiographic imaging methods utilize the attenuation properties of materials (cross sections and thicknesses) to produce a shadow image of the object under investigation (Fig. 23). X-ray and neutron imaging are based upon the same physical principle in that respect. However, since the cross sections of interaction differ considerably, neutron radiography is complimentary to, rather than competitive with, X-ray imaging. Neutron attenuation is governed by the total neutron cross section, which varies irregularly from isotope to isotope, while X-ray attenuation depends on the electron density of the material and therefore increases monotonically with increasing atomic number. Thus, thermal neutrons can visualize hydrogenous material or neutron-absorbing material, even if it is enclosed in metal shields (e.g., lubrication oil in a car engine or the hydrogen bearing rose inside a lead container in Fig. 23). Another field where neutron radiography is the unique method of choice is the quality control imaging of used nuclear fuel elements, which are highly radioactive.

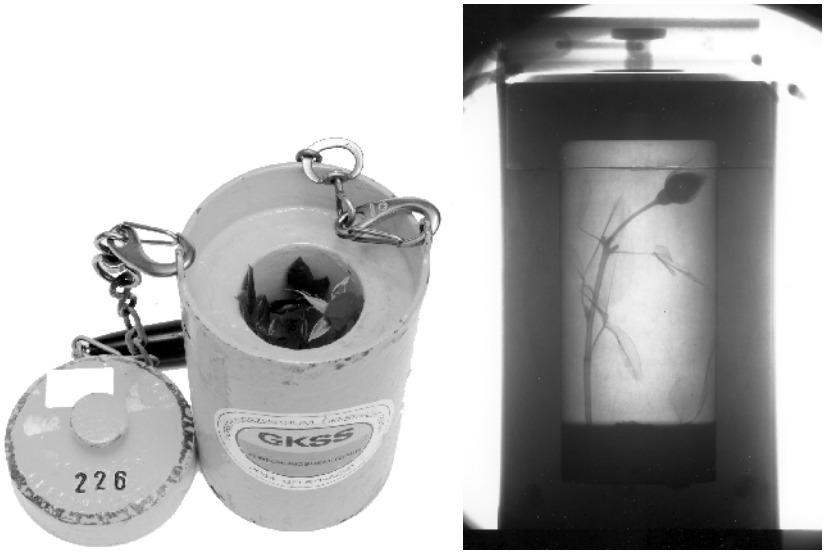

Figure 23. A rose in a lead container used for transporting radioactive materials. The picture to the left shows the setup as a conventional photograph. To the right is a neutron radiography image. The neutrons readily penetrate the lead container and the hydrogen in the rose provides sufficient contrast to see even the leaves of the flower.

The radiography setup is very simple: neutrons emitted by a source are collimated and hit the investigated object, producing a shadow image either on a converter foil or a dynamic neutron detector. The distance from the collimator to the imaging plane L and the pinhole diameter D of the collimator define the so-called collimation ratio L/D, which is an important parameter, since it determines the spatial resolution of the radiograph. Converter foils are sheets of either dysprosium or gadolinium, which by readily absorbing the transmitted neutrons map the image as their excited nuclei emit electrons. The foils are processed using ordinary photographic film. Dynamic detectors enable the investigation of live events, like the distribution of the cooling fluid in a refrigerator or measurement of the rate of descent of a gadolinium sphere in molten rock (Bayon et al. 2001; Winkler et al. 2002). Modern developments of cooled CCD cameras and further development of multi-wire proportional chambers (MPC's) have opened the field of three-dimensional neutron tomography (Schillinger 1996). Using this technique, accurate images for example of metallic mechanical structures and plastic parts within them, or micro-fissures in materials with water intrusion, can be made visible in a non-destructive way. The rose in a lead container in Figure 23 is an example of such an image, showing even the structure of the leaves of the flower. With neutron energies chosen near the Bragg edges of different constituents of poly-crystalline material, phase-specific radiography has been made. Spatial resolutions to date are of the order of 10 μm.

Sample environments

The low attenuation of neutrons by most materials enables the design of special sample environments to measure the response of samples to temperature (typically ~2000 K to a few mK), pressure (vacuum to ~20 GPa), magnetic field (up to 10 T), uni-axial stress (up to ~2 GPa) or combinations of these. Most neutron facilities have beamlines available which provide such sample environments. As an example, Figure 24 shows the SMARTS load-frame/furnace combination, allowing *in situ* deformation of a sample in the neutron beam uni-axially in the horizontal plane (up to 250 kN) while the sample is at a temperature up to 1500 °C (Bourke et

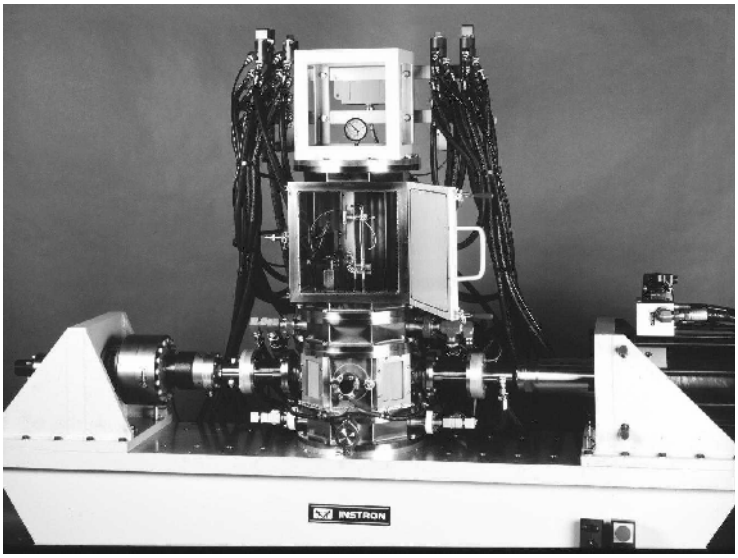

Figure 24. The load-frame/furnace combination of the SMARTS instrument at LANSCE (Bourke et al. 2002).

al. 2002). The changes in peak positions, peak intensities and peak widths provide insight into deformation mechanisms, in particular in combination with modeling approaches (Clausen et al. 1998). Figure 25 gives an example of a recent high pressure cell for neutron diffraction experiments, the ZAP cell. This cell uses a pair of single crystal SiC anvils, from 5 to 100 carats, to apply pressure on a small sample volume (3~30 mm^3) between the anvils. The cell is pre-loaded under high hydraulic loading forces (up to 100 tons) and the hydrostatic pressure is locked into the inner cell. The cell can be removed from the press and then easily transported to experimental setups, such as a neutron diffractometer, where the same sample can be studied under identical pressure-temperature (*P-T*) conditions. The optically transparent windows of SiC anvils are particularly useful for the measurement of vibrational spectra (Raman and IR) on the same sample under identical *P-T* conditions. The straightforward anvil-sample-anvil setting allows applications of acoustic transmission and ultrasonic interferometry techniques for elasticity measurements at high pressures. High pressure neutron scattering techniques are discussed in detail in Parise (2006, this volume). Compared to X-rays, neutrons have the disadvantage for high pressure research that larger sample volumes are required, resulting in larger devices and lower maximum pressures achievable with pressure cells designed for neutron scattering.

Neutrons also allow for *in situ* observation of crystallographic changes under special conditions and environments, such as order-disorder phase transformations (Redfern 2006, this volume), or the change in crystal structure as a function of charge state in a commercial battery (Rodriguez et al. 2004) or during the reduction of $NiAl_2O_4$ to Nickel and Al_2O_3 triggered by a reducing atmosphere (Üstündag et al. 2000). Studies of clathrates (Kuhs et al. 1997; Lokshin et al. 2004; Kuhs and Hansen 2006, this volume) are specific to neutron diffraction since hydrogen is virtually invisible to synchrotron radiation and the required moderate pressures of few kilobars at low temperatures are not achievable with high pressure setups using diamond anvil cells at synchrotron facilities. Figure 26 shows the low temperature pressure cell developed by Lokshin and Zhao (2005).

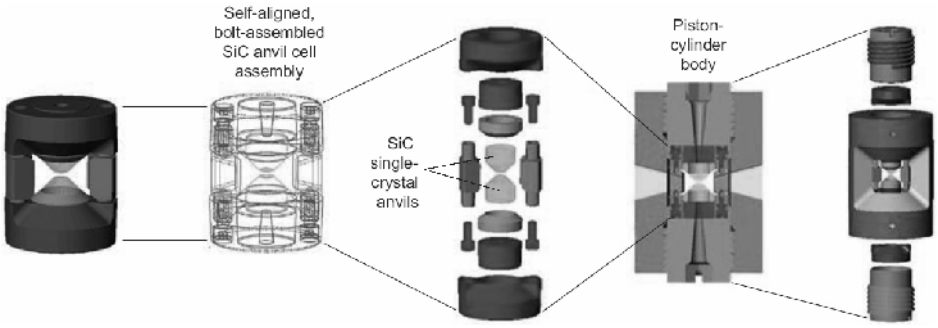

Figure 25. The ZAP cell, a SiC Cell assembly (Migliori et al. 2006).

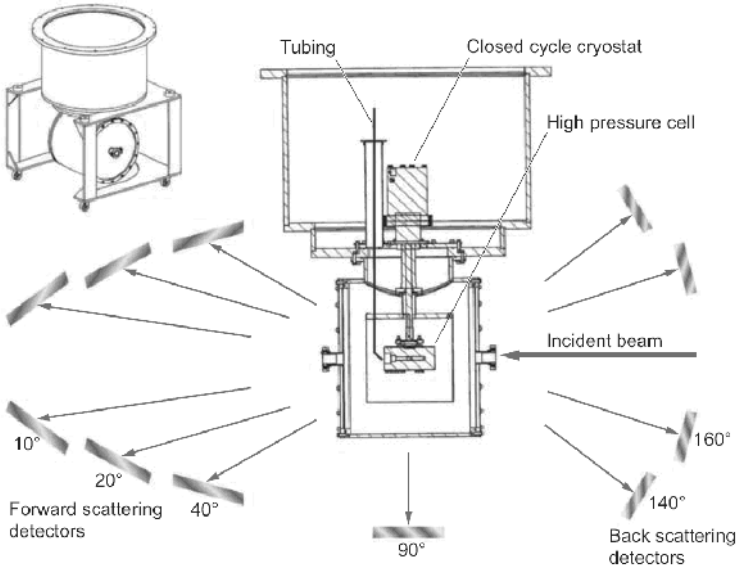

Figure 26. Hydrostatic pressure cell for hydrostatic pressure and low temperature research on HIPPO (Lokshin and Zhao 2005). The outer diameter of the top flange is 0.83 m.

In general, specimen size for neutron experiments is larger (mm^3 to cm^3) than for comparable X-ray or synchrotron measurements (μm^3 to mm^3). This results in negligible artifacts from the surface or sample preparation, and averages the derived information over larger numbers of grains than is possible with X-rays.

NEUTRON DETECTION

To record neutron intensity spectra, neutrons must be converted to charged particles which in turn can be detected electronically. Great care has to be taken to discriminate neutrons from other types of radiation, in particular gamma rays typically present at neutron sources or from cosmic radiation. Due to the low count rates compared to even laboratory X-ray sources, neutron detectors have to be insensitive to gamma radiation. For thermal neutrons, typically scintillation counters or gas counters are employed. Scintillation counters consist of

a scintillator and a photomultiplier (Fig. 27, left). In the scintillator, the neutron absorption according to one of the exothermic reactions

$$^{6}\mathrm{Li} + \mathrm{n} \rightarrow {}^{3}\mathrm{H} + {}^{4}\mathrm{He} + 4.78\ \mathrm{MeV} \tag{21}$$

$$\begin{aligned} {}^{10}\mathrm{B} + \mathrm{n} &\rightarrow {}^{7}\mathrm{Li} + {}^{4}\mathrm{He} + 2.79\ \mathrm{MeV} \quad (6\%) \\ {}^{10}\mathrm{B} + \mathrm{n} &\rightarrow {}^{7}\mathrm{Li}^{*} + {}^{4}\mathrm{He} + 2.31\ \mathrm{MeV} \quad (94\%) \\ &\quad\downarrow \\ &\quad {}^{7}\mathrm{Li} + 480\mathrm{keV} \end{aligned} \tag{22}$$

(where $^{7}\mathrm{Li}^{*}$ designates an excited state of the ^{7}Li nucleus) is followed by the emission of an energetic charged particles which excites atoms of the working medium, causing fluorescent radiation[2]. Some of the emitted light quanta reach the photocathode of the photomultiplier and initiate an electron avalanche which creates a measurable electric charge pulse at the anode. The pulses can be counted, resulting in the desired neutron intensity versus time or diffraction angle histograms. As background radiation, e.g., cosmic radiation or gamma radiation emitted from the neutron source, also causes scintillation, neutrons and other radiation have to be discriminated electronically. This can be performed using the pulse heights and/or the different pulse shapes of the radiation types. Special scintillating glasses, containing lithium enriched in ^{6}Li, such as NE905 or GS20, are commercially available. They can be either glued directly on a photomultiplier tube or cut into small cylinders or cubes of a few mm^2 surface area to form pixelated detectors. In this case, the scintillation light is transmitted through fiber optic light guides to photomultiplier tubes for conversion into electronic signals. Scintillation detectors are the prevalent technology at ISIS.

In a gas counter, helium enriched with ^{3}He, or BF_3 enriched with ^{10}B is placed in a metal cylinder with a thin wire anode (Fig. 27, right). Between the anode and cylinder, a high voltage is applied. Again the neutron is absorbed and according to the above reactions for boron or

$$^{3}\mathrm{He} + \mathrm{n} \rightarrow {}^{3}\mathrm{H} + {}^{1}\mathrm{H} + 0.765\ \mathrm{MeV} \tag{23}$$

fast charged particles are generated. The charged particles are accelerated in the electric field and produce more charged particles by collisions with the gas molecules, generating an avalanche which is converted to an electric pulse at the anode or cathode. The gas counter must be run in the "proportional counter" mode, allowing electronic discrimination of neutrons from gamma ray background by the pulse heights. After discrimination, the pulses may be counted the same way as those of scintillation counters. This type of detectors can be modified to show the location at which a particle arrived, making it a position sensitive detector (PSD). Such neutron detector tubes are available commercially and, for instance, are the standard detectors at IPNS and LANSCE.

In addition to the classical tube setup, so-called microstrip neutron detectors have been developed (Oed 1988): rather than having a potential between a wire in the center of a tube and the tube wall, a grid of strips of alternating potentials is applied to an insulating substrate by means of photolithography. In Figure 28, the potential of the thin conductor strip is positive relative to the two adjacent strips. A charged particle produced in the gas volume above the substrate and reaching this electric field will be accelerated and produce an avalanche amplification. A repulsive electric field is applied from the back of the detector to prevent positive gas ions from accumulating on the insulating substrate surface and degrading the electric field between the strips. This allows production of large position sensitive neutron detectors without dead areas between elements as is the case for detector tubes. The "banana"

[2] The isotope ^{10}B has a natural abundance of about 20%, ^{6}Li of 7.5%.

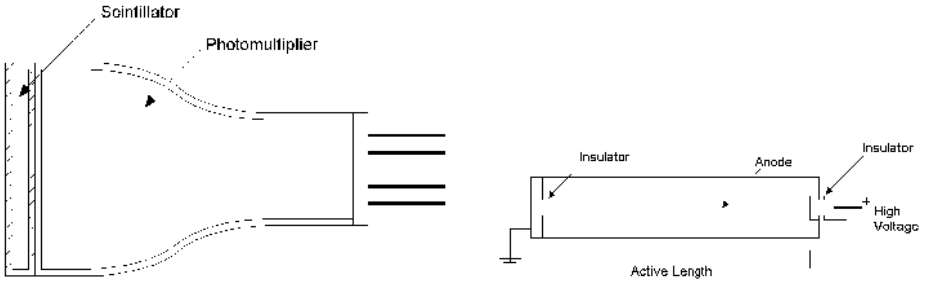

Figure 27. Scintillator/photomultiplier (left) and gaseous proportional counter (right).

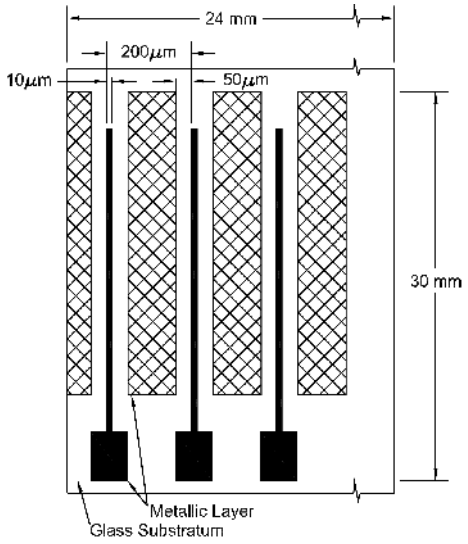

Figure 28. Principle of the position sensitive microstrip detector (Oed 1988).

detectors of the D1B and D20 instruments at ILL are such devices and shown in Kuhs and Hansen (2006, this volume) (Clergeau et al. 2001). Gas counters have, in general, a longer dead time after a detection event compared to scintillation detectors, hence, for instruments with a high event rate at the detector, scintillation detectors might be the only choice. For very fast neutron detection, gas scintillation detectors on the basis of reaction (23) have been developed and are also commercially available.

So-called converter foils (a few microns thickness) use nuclear reactions such as:

$$^{155}\mathrm{Gd} + \mathrm{n} \rightarrow \mathrm{Gd}^{*} \quad \text{and} \quad ^{157}\mathrm{Gd} + \mathrm{n} \rightarrow \mathrm{Gd}^{*} \tag{24}$$

to generate a gadolinium nucleus in an excited state which decays by emission of electrons and/or γ radiation. This radiation can then be detected and integrated using electron or photon detectors such as X-ray or photographic films, CCD cameras, or image plates. Such detectors do not allow discrimination of thermal neutrons against other types of radiation and thus are primarily used for neutron imaging techniques such as neutron radiography or beam alignment studies. The textbook by Knoll (2000) covers most aspects of neutron detection.

HEALTH PHYSICS

Working with nuclear radiation requires precautions to be taken to minimize the exposure of persons involved in an experiment. While facilities in general have issued site-specific rules and codes-of-practice, it is important that the experimenter is familiar with a few facts which help to fulfill the needs of self-control. The radiation types which have to be considered primarily are neutrons, gamma rays and, to a lesser extent, electrons. The biological impact on living organisms depends on the type and energy of the radiation involved: neutrons have a biological effectiveness which is an order of magnitude higher than that of gamma rays and electrons. Because of their absent electric charge, neutrons are readily absorbed by the nuclei of most isotopes, which get into an excited state and release this energy by the emission of electrons and gamma rays. This is why specimens which have spent some time in the neutron beam may have become radioactive and must be monitored before they are removed from an experiment. The intensity of the radiation will decay with time, but the half-lives are very different, depending on isotopes. For instance, 10 g of silver, chlorine, chromium, or potassium exposed for 24 h to the beam on the HIPPO instrument at LANSCE, require about 20 days, 0.1 days, 42 days, and 1.1 days, respectively, to decay to 74 Bq/g (74 disintegrations per second per gram), the limit accepted for shipping material as "non-radioactive." This is the reason why some specimens must stay shielded for a certain time, sometimes for years, in order for the radiation level to drop below the accepted limit. In any case, it is advisable to estimate the expected radiations—types and energies—during the planning phase of an experiment. This will help to comply with the commonly adopted ALARA (as-low-as-reasonably-achievable) principle, which every experimenter should have in mind in order to minimize his or her radiation exposure.

There are a number of ways to shield against nuclear radiation, depending on the type. Neutrons are best shielded by first decreasing their energy, e.g., through scattering in hydrogeneous materials or nuclear inelastic scattering ((n,n′γ) reactions), and then capturing them in ^{6}Li or ^{10}B. Gamma rays interact with electrons and, thus, heavy elements like lead can efficiently be utilized to shield against electromagnetic radiation.

NEUTRONS OR X-RAYS?

Although neutrons have clear advantages over X-rays when studying hydrogen, magnetic structures, phonons, or molecular vibrations, in general, neutrons and X-rays are complementary research tools. Beam time applications and experiments at neutron and synchrotron radiation facilities cost both time and money and many months may transpire between proposal and experiment. As such, care has to be taken that the right tool is used in order to tackle a specific problem. Averaging over sample volumes of a cubic centimeter to cover large numbers of grains for even coarse grained materials might be required, for instance, in re-crystallized metals or rocks to get sufficient grain statistics. In such cases, neutron diffraction with its typically large beam spot sizes and the deep penetration through most materials is the probe of choice. For crystal structure determination, it might be beneficial to use neutrons for studies of compounds consisting of elements of similar atomic numbers or light elements, in particular hydrogen. For more complex structures, the location of certain atoms might be distinguishable by neutrons only, while other atomic species might have good contrast with X-rays and poor contrast with neutrons. In such cases, a combined Rietveld refinement of datasets from both sources may be the best solution (Williams et al. 1988). Isotopic substitution, e.g., D vs. H, allows studies of a specific bond using crystal structure solution and vibrational spectroscopy methods by selectively replacing an isotope in a molecule and investigating the difference in scattering signal.

FURTHER READING

Naturally, a complex topic such as neutron generation and instrumentation cannot be completely covered on a few pages. The textbooks by Bacon (1955), Windsor (1981), Dobrzynski and Blinowski (1994), Byrnes (1996), and Squires (1997), provide further details and in-depth material of the topics covered in this section. The introductory booklets by Pynn (1990) (freely available at *http://www.mrl.ucsb.edu/~pynn/*) and Dianoux and Lander (2003) may serve as entry level literature sufficient for the occasional user of neutron diffraction. A list with links to neutron sources around the world and their user programs can be found at *http://www.ncnr.nist.gov/nsources.html* or *http://idb.neutron-eu.net/facilities.php*.

ACKNOWLEDGMENTS

We wish to thank B. Clausen, J. J. Wall and H.-R. Wenk for valuable comments on this chapter. N. T. Callaway and S. J. Veenis provided Figure 5 and J. J. Wall provided Figures 27 and 28. L. L. Daemen contributed the X-ray diffraction data of CaF_2 in Figure 20. The International Union of Crystallography granted permission to reproduce Figure 16 for this chapter.

REFERENCES

Bacon GE (1955) Neutron Diffraction. Clarendon Press

Bauer GS, Thamm G (1991) Reactors and neutron scattering instruments in western Europe – an update on continuous neutron sources. Physica B 174:476-490

Bayon G, Winkler B, Kahle A, Hennion B, Boutrouille P (2001) Application of dynamic neutron imaging in the earth sciences to determine viscosities and densities of silicate melts. Nondestructive Testing and Evaluation 16:287-296

Berger H (1965) Neutron Radiography - Methods, Capabilities and Applications. Elsevier

Bourke MAM, Dunand DC, Üstündag E (2002) SMARTS – a spectrometer for strain measurement in engineering materials. Appl Phys A 74:S1707-S1709

Bunge HJ, Wenk HR, Pannetier J (1982) Neutron diffraction texture analysis using a 2D position sensitive detector. Textures and Microstructures 5:153-170

Byrnes J (1996) Neutrons, Nuclei and Matter: An Exploration of the Physics of Slow Neutrons. CRC Press

Chen H, Downing RG, Mildner DFR, Gibson WM, Kumakhov MA, Ponomarev IY, Gubarev MV (1992) Guiding and focusing neutron beams using capillary optics. Nature 357:391-393

Clausen B, Lorentzen T, Leffers T (1998) Self-consistent modeling of the plastic deformation of fcc polycrystals and its implications for diffraction measurements of internal stresses. Acta Mater 46:3087-3098

Clergeau JF, Convert P, Feltin D, Fischer HE, Guerard B, Hansen T, Manzin G, Oed A, Palleau P (2001) Operation of sealed microstrip gas chambers at the ILL. Nucl Instrum Methods Phys Res A 471:60–68

Daymond MR (2006) Internal stresses in deformed crystalline aggregates. Rev Mineral Geochem 63:427-458

Detti S, Forsyth VT, Roulet R, Ros R, Tassan A, Schenk, KJ (2004) Comparative neutron and X-ray study of $[PPN][HIr_4(CO)_9(\mu\text{-}Ph_2PCH_2PPh_2)]$. Z Kristallogr 219:47-53

Dianoux AJ, Lander G (2003) Neutron Data Booklet. Old City Publishing

Dobrzynski L, Blinwoski K (1994) Neutrons and Solid State Physics. Ellis Horwood Limited

Donahue JB, Baker GD, Bultman NK, Brun TO, Ferguson PD, Macek RJ, Njegomir MM, Plum MA, Roberts JE, Russell GE, Sommer WF, Tuzel WM (1999) The Lujan Center target upgrade. Transactions of the American Nuclear Society, Accelerator Applications, Long Beach, CA, November 14-18, 1999

Eskildsen MR, Gammel PL, Isaacs ED, Detlefs C, Mortensen K, Bishop DJ (1998) Compound refractive optics for the imaging and focusing of low-energy neutrons. Nature 391:563-566

ESS (2003) European Spallation Source website: *http://www.fz-juelich.de/ess/*

Fermi E, Marshall L (1947) Interference phenomena of slow neutrons. Phys Rev 71:666-677

FRM-2 (2004) Research Reactor Munich II website: *http://www.frm2.tum.de*

Gibson WM, Schultz AJ, Chen-Mayer HH, Mildner DFR, Gnäupel-Herold T, Miller ME, Prask HJ, Vitt R, Youngman R, Carpenter JM (2002) Polycapillary focusing optic for small sample neutron crystallography. J Appl Cryst 35:677-838

Goncharenko IN, Mirebeau I, Mignot JM, Goukasov A (2003) Neutron diffraction on microsamples under high pressures. Neutron News 14:21-25

Goncharenko IN, Mirebeau I, Molina P, Böni P (1997) Focusing neutrons to study small samples. Physica B 234-236:1047-1049
Hurd AJ, Schaefer DW (2006) Introduction to materials and bioscience neutron-scattering research. Los Alamos Science 30:146-151
Hyer DK, Pynn R (1990) LANSCE – a facility for users. Los Alamos Science 19:46-63
Ice GE, Hubbard CR, Larson BC, Pang JWL, Budai JD, Spooner S, Vogel SC (2005) Kirkpatrick–Baez microfocusing optics for thermal neutrons. Nucl Instrum Methods Phys Res A 539:312–320
Ikeda S (2002) Japanese spallation neutron source. Appl Phys A 74:S15-S17
JINR (2005) JINR website: *http://nfdfn.jinr.dubna.su/ibr-2/index.html*
Johnson MR, Kearley GJ, Eckert J (2000) Condensed phase structure and dynamics: A combined neutron scattering and numerical modeling approach. Chem Phys 261:1-274
Johnson MW, Daymond MR (2002) An optimum design for a time-of-flight neutron diffractometer for measuring engineering stresses. J Appl Cryst 35:49-57
Kallmann H (1948) Neutron radiography. Research 1:254-260
Kearley GJ (1995) A review of the analysis of molecular vibrations using INS. Nucl Instrum Methods Phys Res A 354:53-58
King NSP, Ables E, Adams K, Alrick KR, Amann JF, Balzar S, Barnes Jr. PD, Crow ML, Cushing SB, Eddleman JC et al. (1999) An 800-MeV proton radiography facility for dynamic experiments. Nucl Instrum Methods Phys Res A 424:84-91
Knoll GF (2000) Radiation Detection and Measurement. Chapter 14 &15 on Neutron Detection, John Wiley
Kuhs WF, Hansen TC (2006) Time-resolved neutron diffraction studies with emphasis on water ices and gas hydrates. Rev Mineral Geochem 63: 171-204
Kuhs WF, Chazallon B, Radaelli PG, Pauer F (1997) Cage occupancy and compressibility of deuterated N_2-clathrate hydrate by neutron diffraction. J Incl Phen Molec Recog Chem 29:65–77
Lisowski PW (2005) Basic and applied science research at the Los Alamos Neutron Science Center. AIP Conference Proceedings 769:712-717
Lisowski PW, Bowman CD, Russell GJ, Wender SA (1990) The Los Alamos National Laboratory spallation neutron sources. Nucl Sci Eng 106:208-218
Lokshin KA, Zhao Y (2005) Advanced setup for high-pressure and low-temperature neutron diffraction at hydrostatic conditions. Rev Sci Instrum 76:1-4
Lokshin KA, Zhao Y, He D, Mao WL, Mao HK, Hemley RJ, Lobanov MV, Greenblatt M (2004) Structure and dynamics of hydrogen molecules in the novel clathrate hydrate by high pressure neutron diffraction. Phys Rev Lett 93:125503
Loong C-K (2006) Inelastic scattering and applications. Rev Mineral Geochem 63:233-254
Mampe W, Ageron P, Bates JC, Pendlebury JM, Steyerl A (1989a) Neutron lifetime from a liquid walled bottle. Nucl Instrum Methods Phys Res A 284:111-115
Mampe W, Ageron P, Bates JC, Pendlebury JM, Steyerl A (1989b) Neutron lifetime measured with stored ultracold neutrons. Phys Rev Lett 63:593-596
Mansur LK, Gabriel TA, Haines JR, Lousteau DC (2001) R&D for the Spallation Neutron Source mercury target. J Nucl Mater 296:1-16
Mason TE, Abernathy D, Ankner J, Ekkebus A, Granroth G, Hagen M, Herwig K, Hoffmann C, Horak C, Klose F, Miller S, Neuefeind J, Tulk C, Wang XL (2005) The Spallation Neutron Source: A powerful tool for materials research. AIP Conference Proceedings 773:21-25
Mason TE, Arai M, Clausen KN (2003) Next-generation neutron sources. MRS Bull 28:923-928
Mason TE, Crawford RK, Bunick GJ, Ekkebus AE, Belanger D (2002) The spallation neutron source is taking shape. Appl Phys A 74:S11-S14
McIntyre GJ, Melesi L, Guthrie M, Tulk CA, Xu J, Parise JB (2005) One picture says it all - High-pressure cells for neutron Laue diffraction on VIVALDI. J Physics: Condens Matter 17:S3017-S3024
Migliori A, Hurd AJ, Zhao Y, Pantea C (2006) Filling the gap in plutonium properties - studies at intermediate temperatures and pressures. Los Alamos Science 30:86-89
Mitchell PCH, Parker SF, Ramirez-Cuesta AJ, Tomkinson J (2005) Vibrational Spectroscopy with Neutrons. World Scientific Publishing
Oed A (1988) Position-sensitive detector with microstrip anode for electron multiplication with gases. Nucl Instrum Methods Phys Res A 263:351-359
Parise JB (2006) High pressure studies. Rev Mineral Geochem 63:205-231
Pouzo J, Milanese M, Moroso R (2003) Portable neutron probe for soil humidity measurements. AIP Conference Proceedings 669:277-280
Proffen T (2006) Analysis of disordered materials using total scattering and the atomic pair distribution function. Rev Mineral Geochem 63:255-274
PSI (2002) SINQ website: *http://asq.web.psi.ch/ASQ/facilities/SINQSYSTEMS.html*
Pynn R (1990) Neutron scattering – a primer. Los Alamos Science 19:1-31

Radlinski AP (2006) Small-angle neutron scattering and the microstructure of rocks. Rev Mineral Geochem 63:363-397

Redfern SAT (2006) Neutron powder diffraction studies of order-disorder phase transitions and kinetics. Rev Mineral Geochem 63:145-170

Reijonen J, Gicquel F, Hahto SK, King M, Lou TP, Leung KN (2005) D–D neutron generator development at LBNL. Appl Radiat Isot 63:757–763

Richter D (2002) The European spallation source. Appl Phys A 74:S18-S22

Rodriguez MA, Ingersoll D, Vogel SC, Williams DJ (2004) Simultaneous in situ neutron diffraction studies of the anode and cathode in a lithium-ion cell. Electrochem Solid-State Lett 7:A8-A10

Ross NL, Hoffman C (2006) Single-crystal neutron diffraction: present and future applications. Rev Mineral Geochem 63:59-80

Schillinger B (1996) 3D Computer tomography with thermal neutrons at FRM Garching. J Neutron Res 4: 57-63

Schmidt W, Raymond S (2005) CRG - cold neutron three-axis spectrometer IN12. ILL yellow book, *http://www.ill.fr/YellowBook/IN12/*

Shull CG (1995) Early development of neutron scattering. Rev Mod Phys 67:753-757

Squires GL (1997) Introduction to the Theory of Thermal Neutron Scattering. Dover Publications

Stone HJ, Tucker MG, Le Godec Y, Méducin FM, Cope ER, Hayward SA, Ferlat GPJ, Marshall WG, Manolopoulos S, Redfern SAT, Dove MT (2005a) Remote determination of sample temperature by neutron resonance spectroscopy. Nucl Instrum Methods Phys Res A 547:601-615

Stone HJ, Tucker MG, Méducin FM, Dove MT, Redfern SAT, Le Godec Y, Marshall WG (2005b) Temperature measurement in a Paris-Edinburgh cell by neutron resonance spectroscopy. J Appl Phys 98:64905-1-10

Trouw FR (1992) Molecular dynamics simulation and inelastic neutron scattering. Spectrochim Acta A 48: 455-476

Üstündag E, Clausen B, Bourke MAM (2000) Neutron diffraction study of the reduction of $NiAl_2O_4$. Appl Phys Lett 76:694-696

Vogel SC, Hartig C, Lutterotti L, Von Dreele RB, Wenk HR, Williams DJ (2004) Texture measurements using the new neutron diffractometer HIPPO and their analysis using the Rietveld method. Powder Diffraction 19:64-68

Wenk H-R (2006) Neutron diffraction texture analysis. Rev Mineral Geochem 63:399-426

Wenk HR, Lutterotti L, Vogel S (2003) Texture analysis with the new HIPPO TOF diffractometer. Nucl Instrum Methods Phys Res A 515:575-588

Williams A, Kwei GK, Von Dreele RB, Larson AC, Raistrick ID, Bish DL (1988). Joint X-ray and neutron refinement of the structure of superconducting $YBa_2Cu_3O_{7-x}$: precision structure, anisotropic thermal parameters, strain, and cation disorder. Phys Rev B 37:7960-7962

Windsor CG (1981) Pulsed Neutron Scattering. Taylor & Francis

Winkler B (2006) Applications of neutron radiography and neutron tomography. Rev Mineral Geochem 63: 459-471

Winkler B, Knorr K, Kahle A, Von Tobel P, Lehmann E, Hennion B, Bayon G (2002) Neutron imaging and neutron tomography as non-destructive tools to study bulk-rock samples. Eur J Mineral 14:349-354

Withers PJ, Johnson MW, Wright JS (2000) Neutron strain scanning using a radially collimated diffracted beam. Physica B 292:273-285

Womble PC, Campbell C, Vourvopoulos G, Paschal J, Gacsi Z, Hui S (2001) Detection of explosives with the PELAN system. AIP Conference Proceedings 576:1069-1072

Wright AF, Berneron M, Heathman SP (1981) Radial collimator system for reducing background noise during neutron diffraction with area detectors. Nucl Instrum Methods 180:655-658

Xiao QF, Chen H, Sharov VA, Mildner DFR, Downing RG, Gao N, Gibson DM (1994) Neutron focusing optic for submillimeter materials analysis. Rev Sci Instrum 65:3399-3402